J. ISSS Vol. **2** No. 1, pp. 39-71, March 2013.
REGULAR PAPER

MEMS Pressure Sensors- An Overview of Challenges in Technology and Packaging

K. N. Bhat and M. M. Nayak
Centre for Nano Science and Engineering,
Indian Institute of Science,
Bangalore-560012

Keywords:

Pressure sensors
(Low pressure, High pressure),
Microsystems, MEMS,
Silicon Carbide,
Piezo resistors (Si, PolySi, SiC, CNT),
MOS integrated pressure sensors,
Microsystem packaging technology.

Abstract

Pressure sensors are required in all walks of life, irrespective of civilian, defense, aerospace, biomedical, automobile, Oceanography or domestic applications. Naturally, rapid progress has been made in micromachined pressure sensors and the microsystems using these sensors. Starting with metal strain gauges and moving forward with silicon based pressure sensors with flat diaphragms, the search for devices which can operate in harsh environments involving corrosive fluids and high temperatures has spurred activities which lead to pressure sensors using harder materials such as Silicon Carbide (SiC) and Carbon Nano Tubes (CNT). The present article provides an overview of these pressure sensors including their design, engineering, technology and packaging challenges.

1. Introduction

Pressure sensors in their primitive form existed as strain gauges for over several decades. The miniaturization of pressure sensors and other mechanical sensors gained considerable attention soon after the invention of piezoresistivity in silicon and germanium [Smith, 1954]. This activity gained further momentum with the recognition of the excellent mechanical properties of silicon [Peterson, 1982]. The advent of the micromachining of silicon to carve out mechanical microstructures in silicon and the already existing expertise in manufacturing microelectronic devices and integrated circuits in silicon, opened the doors of the highly interdisciplinary area of MEMS and microsystems. During the past two decades, several industries and academic institutions all over the globe have been involved in the development and commercialization of micro sensors for industrial, automobile, defense, space and biomedical applications. Among the various devices, pressure sensors using MEMS technology have received great attention because the pressure sensors find applications in everyday life involving sensing, monitoring and controlling pressure, and they therefore constitute 60 to 70 percent of the market amongst the various MEMS devices.

As the requirements widen, new challenges emerge because the pressures range from a few Pascal (Pa) to several Mega Pascal (MPa) depending on the application and the environment, which vary from being very sensitive in biomedical applications to being very harsh in industrial and automobile applications. Hence, they need to be biocompatible in some applications while they need to be rugged and capable of performing reliably in temperatures well in excess of 80°C to 100°C.They also need to survive in corrosive fluids like ocean water in applications such as Oceanography. In several applications, such as mapping the pressure on the aero foil of an aircraft, the package needs to be flat and the device height needs to be restricted to below a millimeter. Similarly, in biomedical applications such as an intra cranial pressure (ICP)

sensor, where the sensor is inserted into the ventricle, the packaged size should not exceed a diameter of 1mm.

As a result of these several constraints, the packaging of pressure sensors is not a universal technique, and has to be tailor-made depending upon the application. These restrictions on the size of the finished device also impose tremendous constraints on the pressure sensor chip design and fabrication. The demand for pressure sensors over a wide range of pressures varying from a few Pa to several MPa, operation capability at temperatures from -25 ∘C to +125C for aerospace applications and the growing demand for pressure measurements in high-temperature environments (>500 °C) have spurred the development of robust, reliable MEMS-based pressure sensor technologies involving silicon, Silicon on Insulator (SOI), Silicon on Sapphire (SOS), Silicon Carbide (SiC) and Carbon Nanotubes (CNT). As a result, the constraints and the capability requirements on the ruggedness of the microsystem packaging technology have been tremendous.

This paper aims at providing an overall scenario of pressure sensor technology, beginning from basic principles. This is followed by design criteria for different ranges of pressures and the related technology, based on silicon as the diaphragm material and piezoresistor, SOI and polysilicon piezoresistors for higher temperatures and high pressures followed by more exotic materials like SiC and CNT for capacitive and piezoresistive pressure sensors. The paper elucidates the use of bossed structures, which result in sculptured diaphragms for low-pressure applications with greater linearity. The paper also gives a glimpse of some of our work which has been supported by the NPMASS program at the Centre for Nano Science and Engineering (CeNSE) at IISc and includes a section on the challenges of reliable pressure sensor packaging technology for operation in harsh corrosive environments.

2. Pressure Sensor Types and Classification

Pressure sensors are categorized as absolute, gauge and differential pressure sensors based on the reference pressure with respect to which the measurement is carried out. Particular applications are as follows.

(a) Absolute Pressure Sensors measure the pressure relative to a reference vacuum encapsulated within the sensor as shown in Figure 1. Such devices are used for atmospheric pressure measurement and as manifold absolute pressure (MAP) sensors for automobile ignition and airflow control systems. Pressure sensors used for cabin pressure control, launch vehicles, and satellites also belong to this category.

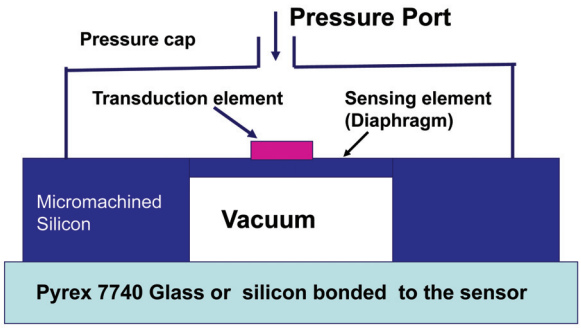

Fig. 1 Schematic diagram of Absolute Pressure sensor

(b) Gauge Pressure sensors measure pressure relative to atmospheric pressure. One side of the diaphragm is vented to atmospheric pressure as shown in Figure 2. Blood pressure (BP), intra-cranial pressure (ICP), gas cylinder pressure and most of ground-based pressure measurements are gauge pressure sensors. Vacuum sensors are gauge sensors designed to operate in the negative pressure region.

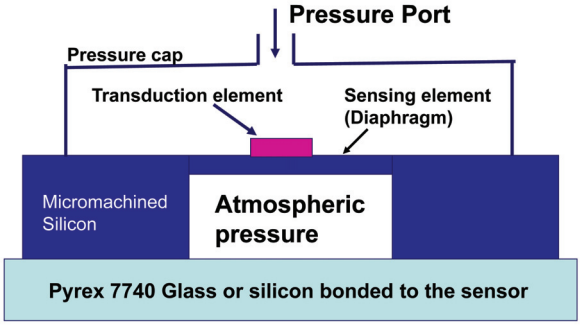

Fig. 2 Schematic diagram of Gauge Pressure sensor

(c) Differential Pressure Sensors measure accurately the difference ΔP between two pressures P1 and P2 across the diaphragm (with ΔP << P1 or P2), and hence need two pressure ports as shown in Figure 3. They find applications in airplanes used in warfare. They are also used in high pressure oxidation systems where it is required

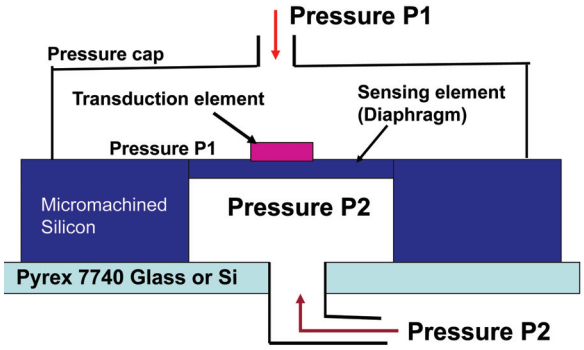

Fig. 3 Schematic diagram of Differential Pressure sensors

to maintain an oxygen pressure ranging from 1 to 10 atmospheres inside a quartz tube during the oxidation of silicon. In this system, the outside of the quartz tube is maintained at a slightly higher gas pressure of nitrogen, and the pressure difference is monitored using a differential pressure sensor which ensures that the quartz tube does not experience a differential pressure greater than its rupture stress of 1 atmosphere (10^5 Pascal). The differential pressure sensor is also used in some applications where it is desirable to detect small differential pressures superimposed on large static pressures.

In almost all types of pressure sensors, the basic sensing element is the diaphragm, which deflects in response to the pressure. As the deflections in diaphragm-based sensors are small they cannot be directly measured. This mechanical deflection or the resulting strain in the diaphragm is converted ultimately into electrical signals using suitable transduction mechanisms, namely, capacitive, piezoresistive or piezo-electric techniques, which are usually employed as adjectives for the pressure sensors as described below:

(i) Strain gauges and Piezoresistive pressure sensors: In traditional metal diaphragm-based pressure sensors, the most common method has been to locate metal strain gauges (foil type) on the metal diaphragm, in positions of maximum stress to maximize the sensitivity. With the invention of piezo-resistivity in Silicon, and silicon micromachining for diaphragm realization, boron-doped silicon piezoresistors have replaced the metal strain gauges. In this approach, much higher sensitivities have been achieved because the piezo-resistors are embedded directly on the silicon diaphragm by implanting or diffusing boron in the selected regions of maximum stress as shown in Figure 4(a). These resistors are connected in the form of a Whetstone Bridge which gives an output when the resistors are strained under the action of the pressure sensed by the diaphragm. It will be seen in subsequent sections that piezoresistive pressure sensors enable linear operation over a wide range of pressures. They are also simple to fabricate. As a result, they have captured the major market of pressure sensors encompassing the automobile industry, defense, space as well as biomedical applications.

Other transduction techniques are capacitance and piezoelectric approaches and they are identified as capacitive pressure sensor and piezoelectric pressure sensors respectively.

(ii) **Capacitive Pressure Sensor**: A schematic diagram of a silicon micro machined sensor of this type is shown in Figure 4(b).This approach uses the diaphragm as one electrode of a parallel plate capacitor structure and diaphragm displacement causes a change in capacitance with respect to a fixed electrode. The merits of capacitive pressure sensors are their high sensitivity, which is practically invariant with temperature. However, in this case, an electronic circuit is required to convert the

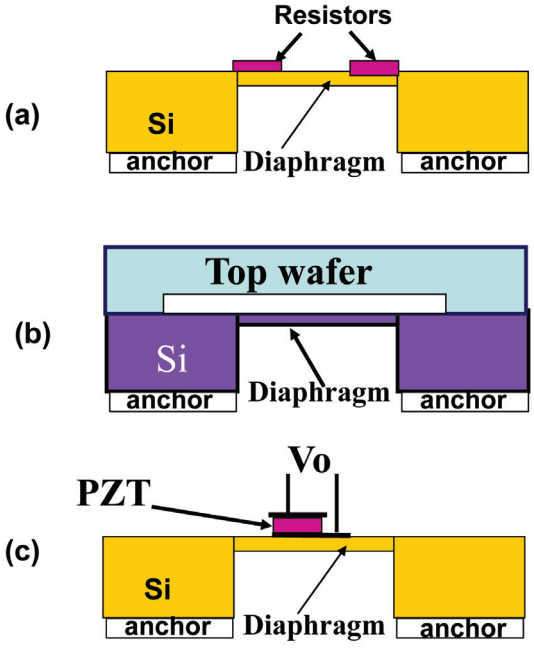

Fig. 4 Schematic representation of micrmachined silicon pressure sensors (a) Piezoresistive (b) capacitive (c) Piezoelectric

capacitance change into an electrical output. An additional disadvantage of this approach is the nonlinear relationship between the capacitance and displacement and hence a force-balancing and linearizing electronic circuit is essential to capture a wide range of pressures.

(iii) Piezoelectric pressure sensors: Silicon does not show a piezoelectric effect. Therefore, a piezoelectric sensing element, such as Lead Zirconate Titanate (PZT) or Zinc Oxide (ZnO) are placed/deposited on to the silicon diaphragm as shown in Figure 4(c). The deflection of the diaphragm induces strain in the piezoelectric material and hence a charge is generated. These sensors are only suitable for measuring dynamic pressures and are not suitable for static pressure sensing because piezoelectric materials only respond to changing strains. The major advantage of this approach is that an external power supply is not required.

In another approach, in which pressure sensors are identified as **resonant sensors,** the vibration frequency of a mechanical beam or a membrane, which depends on the extent to which it is stretched, is used This is similar to the vibration frequency of a violin string. The output signal from a resonant sensor is a frequency, which can easily be transferred into a digital signal and interfaced with computer systems, without having to use an Analog to Digital converter. In most of the cases, a quartz resonating beam is used because these sensors are noted for their high stability and high resolution as a frequency signal is much more robust than an amplitude (e.g. a voltage). The stability is determined only by the mechanical properties of the resonator material, which is generally very stable. On the flip side, resonant silicon sensors are not easy to fabricate and hence become expensive. The high costs may be compensated by innovative simpler mechanical structures and by simpler electronics.

In all the types of pressure sensors, the diaphragm is invariably, if not always, chosen as the sensing element. The static and dynamic performance characteristics of the diaphragm are of great importance and provide suitable design guidelines for designing pressure sensors. These aspects of micromachined diaphragms are discussed in the following section.

3. Static and Dynamic Analysis of Micromachined Si Diaphragms

3.1 Linear Range of Operation

The diaphragm design is the most crucial step among the various stages of pressure sensor realization. The dimensions of the diaphragm need to be chosen to ensure linearity of operation over the entire pressure range of operation of the sensor. In most situations, the diaphragms of the pressure sensors turn out to be square or rectangular in the lateral direction while being rigidly anchored at the edges, as shown in Figure 5. Consider a square diaphragm of thickness h and side length = $2a$, subjected to a uniform pressure P. From the theory of plates [Meleshenko, 1997], the maximum deflection at the center of the diaphragm is given by the equation,

$$P = E\,\frac{h^4}{a^4}\left[g_1 \frac{w_0}{h} + g_2 \left(\frac{w_0}{h} \right)^3 \right] \qquad (1)$$

Where E is Young's modulus and g_1 and g_2 are constants related to Poisson's ratio, ν, by the relation

$$g_1 = \frac{4.13}{1-\nu^2} = 4.54, \qquad g_2 = \frac{1.98(1-0.585\nu)}{1-\nu} = 2.33$$

Substituting v = 0.3 for silicon, g_1 and g_2 turn out to be 4.54 and 2.33 respectively. Thus the maximum deflection w_o is linearly related to pressure P till w_o <<h. The second term inside the bracket is about 0.5 % of the first term when w_o = 0.1h and the deflection w_o in the linear region of operation can be expressed as follows for a square diaphragm

$$\frac{w_o}{h} = \frac{Pa^4}{Eh^4 g_1} \qquad (2)$$

Using (2) for a square diaphragm, of silicon (E=170GPa), with side length $2a$ = 500 μm and thickness h=10 μm, the maximum deflection is estimated to be 0.5 μm when P=10^5 Pascal = 1bar.

The maximum stress σ_{max}, which occurs in the middle at the edge of the square diaphragm (ie,

at $x = \pm a$ in Figure 5), can be expressed by the analytical expression for a square diaphragm as,

$$\sigma_{max} = P\left(\frac{a}{h}\right)^2 \qquad (3)$$

The stress distribution on the top surface of a rectangular diaphragm of side lengths $2a$ and $2b$ shown in Figure 5 are estimated with FEM techniques using the commercial simulator ANSYS. The results of a simulation study [Bhat et al., 2005] undertaken for a rectangular diaphragm, with the aspect ratio L/W ranging from 1 to 2, are presented in Figure 6, which shows the longitudinal stress component along the x-direction as x is varied from $-a$ to $+a$ along the dotted line shown in Figure 5. In this study the width $w = 2a$ is kept fixed at $2a = 500$ µm and the diaphragm thickness h is held at 10µm.The simulation was carried out with the diaphragm subjected to a uniform pressure P=3bar directed perpendicularly into the top surface of the diaphragm as shown in Figure 5. It is evident, from the results in Figure 6, that the x-component of the stress is tensile and is greatest at the middle of the diaphragm edges. This stress component decreases as one moves towards the center of the diaphragm, becomes zero and then changes to compressive

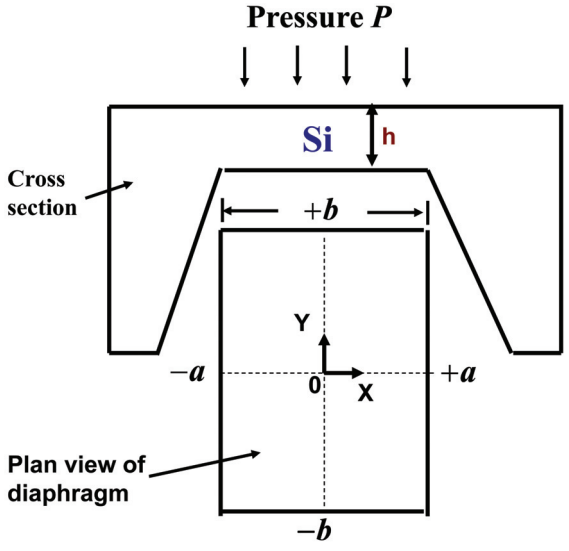

Fig. 5 Micromachined rectangular diaphragm of silicon showing the cross section and the diaphragm plan view

stress at the center of the diaphragm where the compressive stress takes a maximum magnitude. Similarly, Figure 7 presents [Bhat et al., 2005] the transverse stress component in the y-direction, as x is varied from $-a$ to $+a$. For a piezoresistive pressure sensor, the locations of maximum tensile and compressive stress on the diaphragm surface are important to achieve the maximum sensitivity by placing the resistors in those locations. Figures 8 and 9 show these longitudinal and transverse stress components respectively at the diaphragm edge (x=±a, y=0) and at the center (x=0, y=0) for

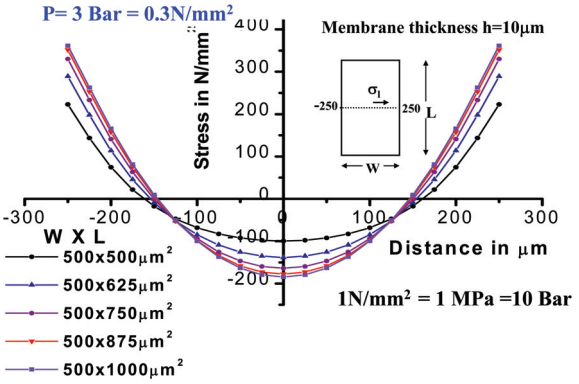

Fig. 6 ANSYS simulation results on longitudinal Stress across a diaphragm for different aspect ratios [Bhat et al, 2005].

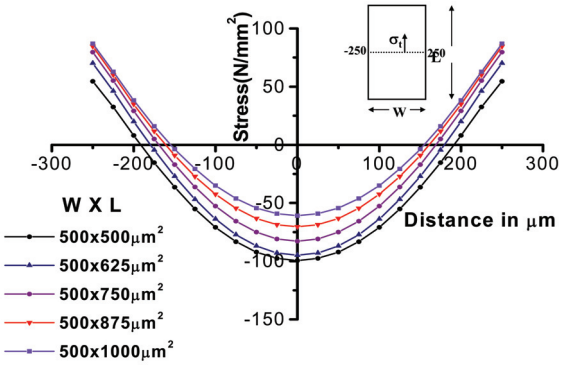

Fig. 7 ANSYS simulation results on transverse Stress across a diaphragm for different aspect ratios [Bhat et al, 2005]

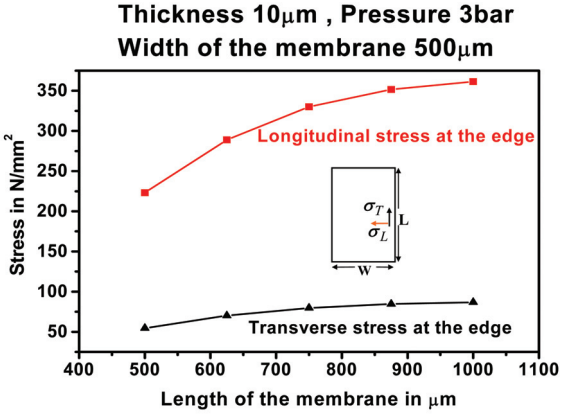

Fig. 8 Longitudinal and transverse stress in he middle at the diaphragm edge [Bhat et al, 2005].

different magnitudes of the diaphragm length, L ranging from 500 µmto1000µm [Bhat et al., 2005], for the case h=10µm and the width, W=2a=500µm, when the uniform applied pressure is P=3bar. In both the figures, the positive signs indicate that the stress is in the same direction as marked in the inset in these figures. The negative signs indicate that the stresses are opposite in direction to that marked in the inset figure.

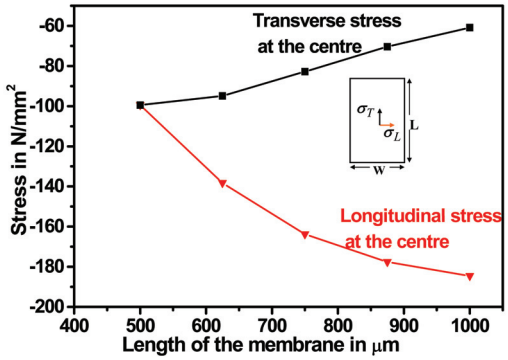

Fig. 9 Longitudinal and transverse stress at the center of the diaphragm [Bhat et al, 2005].

The analysis above demonstrates that for a given diaphragm thickness h, and pressure, the longitudinal tensile stress component (indicated by the positive sign) at the diaphragm edge as well as the longitudinal compressive stress (indicated by the negative sign) at the diaphragm center (x=0, y=0) increase with an increase in the aspect ratio (L/W) of the diaphragm, and that both of them almost saturate when L/W is 2. These criteria need to be considered while designing the piezoresistor size and its location on the chip.

3.2 The Proof Pressure and Burst Pressure

The proof pressure is normally defined as 1.5 times the nominal pressure of the sensor. The sensor is required to operate up to this pressure while maintaining the overall specifications. Burst pressure is another important design consideration for the diaphragm dimensions, because this limits the ultimate stress to which the diaphragm can be subjected. This is the pressure at which the maximum stress σ_{max} on the diaphragm becomes equal to the critical stress σ_c which is actually the yield strength of the material. For the case of a single crystal silicon, σ_c=7GPa. Thus, for a square diaphragm having side length $2a$ and thickness, h, the burst pressure P_B is determined by substituting $\sigma_{max}=\sigma_c$ in equation (3) and can be written as in (4).

$$P_B\left(\frac{a}{h}\right)^2 = \sigma_c \qquad (4)$$

As the magnitude of maximum stress is higher in rectangular diaphragms, the burst pressure of the diaphragms having (L/W) > 1 is lower than the corresponding square diaphragm having (L/W) =1. This can, indeed, be seen from the ANSYS simulation results [Bhat et al., 2005] presented in Figure 10 for rectangular diaphragms of three different thicknesses with a diaphragm width W=2a=500µm. On considering a diaphragm of thickness h=10 microns, the burst pressure is reduced from 95 bar to 65 bar when the diaphragm length, L, is varied from 500µm to 1000µm.

3.3 Dynamic Response of the Pressure Sensor

Apart from static response and sensitivity, the frequency response of the pressure sensor is an important parameter which becomes important in situations where it is required to monitor the changes in pressure over small intervals of time, as in the case of blood pressure (BP) or Intracranial pressure (ICP) monitoring. The frequency response indicates the ability of the sensing system to precisely respond to dynamic changes in pressure. The frequency response is governed by the sensing element which acts like a spring –mass system. The natural frequency of silicon micromachined pressure sensors is generally high because of their small size and high Young's modulus of silicon. Based on the theory of plates [Timoshenko & Woinowski-Krieger 1983], the resonance frequency of a clamped square diaphragm is given by the relation involving the diaphragm thickness h, width 2a, the material properties, namely, Young's modulus E and the density ρ, as follows:

$$f_r = 1.65\frac{h}{a^2}\sqrt{\frac{E(1-\nu^2)}{\rho}} \qquad (5)$$

For a square diaphragm with 2a= 0.5mm and thickness 10 µm the resonance frequency is estimated to be 2.15MHz. Thicker diaphragms in higher pressure sensors give proportionately higher resonance frequencies. Figure 11 shows some of

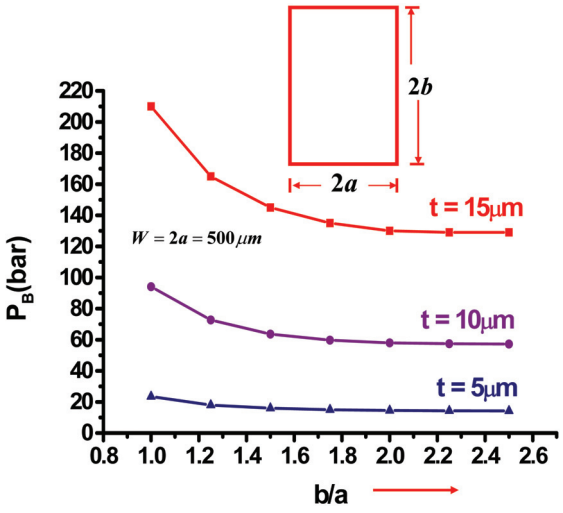

Fig. 10 Burst Pressure P_B versus diaphragm aspect ratio for fixed width=500mm [Bhat et al., 2005].

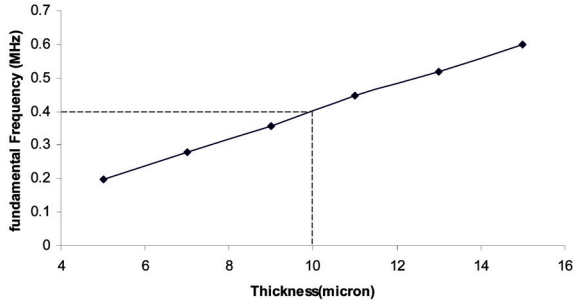

Fig. 11 Resonance frequency of rectangular diaphragms having different thickness lateral dimension of 1mmx0.5mm

the results obtained using ANSYS simulations of rigidly clamped rectangular diaphragms of different thickness. It can be seen from this simulation that the resonance frequency of 400kHz can be achieved using a 1mm x 0.5mm rectangular diaphragm with 10μm thickness. This gives the micro machined silicon diaphragm excellent inherent dynamic response characteristics.

However, when isolation of the diaphragm from a pressurized environment is required, a stainless steel barrier diaphragm is employed between the pressure sensor and the pressurized media. The volume between the steel diaphragm and the silicon sensor is filled with hydraulic oil that transmits the pressure to the sensor die. This additional barrier between the pressurized media and the sensor has a dampening effect and hence lowers the resonance frequency of the sensor as a whole.

4. Piezoresitive Transducer Analyses and Design

Among the various types of pressure sensors, piezoresistive pressure sensors and piezoelectric pressure sensors work on the principle of converting the strain developed on the sensor chip into change in resistance and voltage respectively. Therefore, the sensitivity of these two types of pressure sensors is governed by the location of maximum stress regions on the chip when the diaphragm is subjected to pressure. On the other hand, the performance of capacitive sensors is judged by the extent of change in the capacitance of a movable electrode with respect to a fixed reference electrode. Therefore, the operation range and sensitivity of the capacitive sensor is determined (i) by the extent to which the electrode can deflect, (ii) the ability to minimize stray capacitances and (iii) capacitance voltage conversion circuits.

Due to their simplicity of fabrication and the wide range of pressures, ranging from a few kPa to several hundreds of kPa over which they can perform with excellent linearity and accuracy, piezoresistive pressure sensors have received maximum attention and acceptance in automobiles, airplanes, missiles, and rockets as well as in biomedical applications. Therefore, in this section, we consider the various design criteria and fabrication process steps involved in the development of piezoresitive pressure sensors. Following the diaphragm design and identification of the regions of high stress components on the diaphragm, the next important design parameter is the design of resistors and their dimensions.

In the following sections, we first focus on various parameters such as the gauge factor and piezorestive coefficient and the factors influencing their magnitudes, and hence, the sensitivity of the piezoresistive pressure sensors

4.1 The Gauge Factor and the Piezoresistive Effect

The piezoresistive effect can be quantified using the gauge factor which is defined as the ratio of the relative change in resistance ($\Delta R / R$) when the resistor is subjected to a strain, ε, and is expressed by the relation,

$$G = \frac{\Delta R}{R\epsilon} \tag{6}$$

The resistance R of a rectangular resistor of length L, width W, thickness H and the resistivity, r, is expressed by the relation,

$$R = \frac{\rho L}{WH} \tag{7}$$

When the resistor is subjected to strain, the following relation gives the relative change in resistance ($\Delta R/R$).

$$\frac{\Delta R}{R} = \frac{\Delta L}{L} - \frac{\Delta W}{W} = \frac{\Delta H}{H} + \frac{\Delta \rho}{\rho} \tag{8}$$

Here ΔL, ΔW, ΔH and $\Delta \rho$ are the changes in the respective parameters due to the strain. If the resistors experience tensile stress along their length, the thickness and width of the resistors will decrease whereas the length will increase. Using Poisson's ratio, ν, the change, ΔL, in length is correlated to the change, ΔW in width, and the change, ΔH, in thickness of the piezoresistors by the following equation

$$\frac{\Delta W}{W} = \frac{\Delta H}{H} = -\nu \frac{\Delta L}{L} \tag{9}$$

Combining equations (8) and (9), and using the definition given in (6), the gauge factor G is obtained as:

$$G = \frac{\Delta R}{R\epsilon} = 1 + 2\nu + \frac{\Delta \rho}{\rho \varepsilon} \tag{10}$$

where $\varepsilon = \frac{\Delta L}{L}$ is the strain. The first two terms in equation (10) represent the change in resistance due to dimensional changes and are dominant in metal gauges, while the last term is due to a change in resistivity. Table -1 gives the gauge factors of different types of strain gauges.

Thus the gauge factors of different types of strain gauges can be vastly different. This is mainly due to the difference in the extent of the resistivity, ρ, change under the influence of strain. For metals, ρ does not vary significantly with strain and Poisson's ratio, ν, is typically in the range of 0.3 to 0.5, leading to gauge factors of only about 2 to 5 in metal strain gauges. In semiconductor strain gauges, the piezoresistive effect, which causes large changes in ρ is dominant and hence the gauge factor is considerably high. Gauge factors up to 200 for P-type silicon and up to 140 for N-type silicon have been reported.

Table-1. Gauge factors of different types of strain gauges [Kovacs 1998; Mosser et al., 1991]

Type of Strain Gauge	Gauge Factor
Metal Foil	1 to 5
Thin-Film Metal	≈ 2
Diffused Semiconductor	80 to 200
Polycrystalline Silicon	≈ 30
Polycrystalline SiC	3 to 5
Single crystal SiC	10 to 30
Carbon Nano Tube (CNT)	200 to 1000

It may be noted that in metal strain gauges, the gauge factor is small and in the range 1 to 5 because in metals the change in the resistance due to strain is mainly attributed to a change in physical dimensions. On the other hand, gauge factors in the range of 80 to 200 have been observed in diffused semiconductor resistors. This is attributed to the **piezoresistive effect,** which results in large change in the resistivity (ρ) in semiconductors, whereas in metal foils and thin film metals the change in resistivity is very small. From Table-1, it can also be seen that Carbon Nano Tubes (CNT) show a very high gauge factor close to even 1000, and this has recently led to research that uses CNT as the piezoresistive element instead of silicon

4.2 Atomistic Model for the Piezoresistive Effect in Semiconductors

Piezoresistivity in silicon is usually explained based on the deformation of energy bands as a result of stress. This affects the effective mass, and consequently the mobility of electrons and holes, and hence, modifyies the resistivity. However, a qualitative model based on an atomistic model of a semiconductor provides a more physical explanation to account for the piezoresistive effect in both P-type and N-type semiconductors. In this model, the effect of scattering due to changes in the mean free path is considered to account for the change in

mobility. This model is presented below for both N-type and P-type materials.

(i) N-type semiconductor: When an N-type semiconductor resistor is stretched along its longitudinal direction, the lattice spacing increases by a small extent causing the lattice scattering mean free path length to increase, thus reduces the probability of the scattering of electrons by the lattice atoms, thus leading to an increase in electron mobility. This causes a reduction in resistivity, ρ, which varies inversely as the mobility μ_n as given by the relation,

$$\rho = \frac{1}{q\mu_n n} \tag{11}$$

where q is the electron charge and n is the electron concentration. Similarly when the N-type resistor is subjected to longitudinal compressive stress the mean free path decreases, causing an increase in the scattering probability, thus leading to a reduction in μ_n and hence an increase in resistivity, ρ.

In metals, as the atoms are more closely packed, the change in the mean free path and hence the change in mobility is not noticed particularly because the electron concentration in metals is several orders higher than in semiconductor resistors.

(ii) **P-type semiconductor:** Consider a P-type semiconductor resistor, when it is stretched along its longitudinal direction. In the atomistic model of semiconductors the hole transport in a P-type semiconductor takes place by the jump movement of electrons from an occupied site to a nearby vacant site on the lattice atom. The distance between the lattice atoms increases by a small extent when the lattice is stretched; hence, the electron jump to the nearby lattice becomes more difficult. This, indeed, hampers the hole transport and appears to increase its effective mass and hence, lowers hole mobility. This leads to an increase in the resistivity of P-type resistors when subjected to longitudinal tensile stress. By the same argument, it can be seen that the resistivity of the P-type semiconductor resistor falls when subjected to longitudinal compressive stress. The resistivity of the P-type semiconductor is given by equation (11) replacing electron concentration n with hole concentration p, and electron mobility with hole mobility .

4.3 Piezoresistive Coefficients

The resistance change can be calculated as a function of stress using the concept of the piezoresistive coefficient. Contributions to the resistance change come from longitudinal stress (σ_L) and transverse stress (σ_t) with respect to the current flow. Assuming that mechanical stresses are constant over the resistors, the resistance change ΔR with respect to the resistance R is given by,

$$\frac{\Delta R}{R} = \sigma_L \pi_L + \sigma_t \pi_t \tag{12}$$

Where π_L and π_t are the longitudinal and transverse piezoresistive coefficients, respectively.

Table-2 shows the piezoresistive coefficients [Middlelhoek & Audet, 1989] for N-type and P-type {100} silicon and doping levels below 10^{18} $cm^{-3.}$ The values decrease at higher doping concentrations. For {100} wafers, the piezoresistive coefficients for P-type elements are maximum in the <110> directions and are zero along the <100> directions. Therefore, P-type piezoresistors must

Table-2 Piezoresistive coefficients for (100) Si and doping density less than 10^{18} / cm^3 [Middlelhoek & Audet, 1989]

Silicon type	Orientation of resistor	$\pi_1(10^{-11}$ / Pa)	$\pi_t(10^{-11}$ / Pa)
P-type	In <100> Direction	0	0
P-type	In <110> direction	72	-65
N-type	In <100> Direction	-102	53
N-type	In <110> direction	-32	0

be oriented along the <110> directions to measure stress. Because of the higher piezoresitive coefficients in P-type resistors, most piezoresistive pressure sensors employ P-type resistors on (100) wafers and align them in the <110.>directions.

5. Single Crystal Piezoresistive Pressure Sensor with Flat Diaphragms

A micromachined piezoresistive pressure sensor makes use of a square or rectangular diaphragm of N-type silicon, which acts as the sensing element. Figures 12(a) and (b) respectively, show the cut away isometric view, and the top view of the piezoresistive pressure sensor. The Four P-type piezoresistors equal magnitude, marked R_1, R_2, R_3 and R_4 for identification, are embedded on to this diaphragm by ion implantation or by the diffusion of boron. They are then laid out as shown and are connected in a Wheatstone bridge configuration as shown in Figure 12(c). PN junctions formed by individual P-type resistors with the N-type diaphragm provide the isolation required between the resistors. Though it would be preferable to use circular diaphragms to prevent unwanted stress concentration, silicon diaphragms turn out to be square or rectangular when they are fabricated using anisotropic wet chemical etching on silicon wafers of <100> orientation. It is also easier to align the resistors parallel and perpendicular to the edges of the diaphragm which are in the <110> direction, thus ensuring that the piezoresistive coefficients π_l and π_t are maximum along this direction.

5.1 Diaphragm Design

In miniaturized pressure sensors, the lateral dimension has an upper limit. For instance, in biomedical applications such as intra-cranial pressure monitoring, the chip size needs to be kept below an upper limit of 1mmx1mm. This limits the diaphragm size to below 500μm. Once this lateral dimension is finalized, the thickness of the diaphragm can be chosen based on linearity and burst pressure conditions.

As discussed in Section-3, the maximum operating pressure is limited by two parameters (a) the linearity limit and (b) the burst pressure limit. The linearity limit can be arrived at using equation (1). In this equation, the first term is due to the stress distribution caused by pure bending when the central plane of the diaphragm is not stretched or compressed. This is true if the deflection,w_o, of the diaphragm is small compared to its thickness, h. If w_o is not small when compared to h, the central plane of the diaphragm will be stretched like a balloon. The second term in this equation represents the stress caused by the stretching of the central plane and makes the deflection nonlinear with respect to the pressure. Therefore, even though a reduction in thickness would increase deflection w_o, and hence, the sensitivity of the pressure sensor, it is necessary to keep h sufficiently thick so that w_o at the maximum operation pressure is small when compared to h. The burst pressure limit for a square diaphragm is determined using equation (4). This limit would come into the picture at a much higher pressure compared to the linear limit on the thickness for a given size of the diaphragm. It may also be noted from Figure 10 that for a given thickness of the diaphragm, the burst pressure becomes lower when the diaphragm aspect ratio b/a is increased. In general, the diaphragm dimensions (thickness and aspect ratio) are so chosen that the proof pressure is below one fifth of the burst pressure (P_B/5), further guided by the permitted nonlinearity.

5.2 Positioning the Piezoresistors for Best Sensitivity

The proper positioning of the piezoresistors on the diaphragm needs to be chosen to achieve the best sensitivity with the diaphragm dimensions designed according to linearity and burst pressure considerations. In the case of a single crystal piezoresistive pressure sensor, the four diffused or implanted P-type piezoresistive transducer elements are embedded near the edge of the diaphragm, as shown in Figure 12(b), where the stress is maximum as seen by the simulation results in Figure 6. Here, the two piezoresistors R_1 and R_3 are placed parallel to opposite edges of the membrane, and the other two resistors R_2 and R_4 are placed perpendicular to the other two edges. When a uniform pressure is applied on the back surface as shown in Figure 12(a), the diaphragm deflects upwards, causing compressive stress at the edges of the membrane surface. This causes the resistors R_1 and R_3 to experience transverse

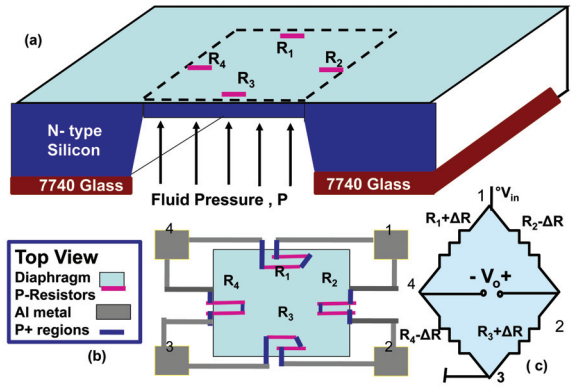

Fig. 12 Silicon micromachined pressure sensor

compressive stress and the longitudinal tensile stress given by the relations (the negative sign on is indicative of compressive stress).

$$\sigma_t = -P\frac{a^2}{h^2}\text{, and } \sigma_l = \nu P\frac{a^2}{h^2} \qquad (13)$$

Hence they show an increase in resistance ΔR given by the relation,

$$\frac{\Delta R}{R} = \pi_t P\frac{a^2}{h^2}(1-\nu) \qquad (14)$$

Similarly the resistors R_2 and R_4 laid out perpendicular to the edge of the diaphragm experience longitudinal and transverse stresses given by,

$$\sigma_l = -P\frac{a^2}{h^2}\text{, and } \sigma_t = \nu P\frac{a^2}{h^2} \qquad (15)$$

and they show a decrease in resistance given by the relation

$$\frac{\Delta R}{R} = -\pi_l P\frac{a^2}{h^2}(1-\nu) \qquad (16)$$

In single crystal (100) silicon, π_l and π_t are equal to each other in magnitude. Therefore, the maximum sensitivity can be achieved when the four resistors fabricated by diffusion on to a single crystal silicon diaphragm are arranged in locations as shown in Figure 12. All the four resistors, (R_1, R_2. R_3 and R_4), are chosen to be equal in magnitude so that the bridge is balanced when the v 0pressure is zero. When the diaphragm is subjected to uniform pressure, P, an imbalance is created in the bridge which gives rise to an electrical output $v_0$of polarity shown in Figure 12(c) for the applied voltage V_{in} and is given by the relation,

$$V_0 = \frac{\Delta R}{R}V_{in} = P\frac{a^2}{h^2}(1-\nu)\pi_l V_{in} \qquad (17)$$

Where R is the zero-stress resistance of each of the resistors.

Equation (17) is derived based on the simplifying assumption that the magnitude of transverse stress on the resistors marked R_1 and R_3 is the same as the magnitude of longitudinal stress on the resistors marked R_2 and R_4, so that the ΔR is same in magnitude on all the four resistors. In practice, this is not true because, as can be seen from Figure 6, the average longitudinal stress on the resistors R_2 and R_4 would decrease along its length considerably, whereas the variation in the stress along the length of the resistors R_1 and R_3 is rather small. The stress variation along the length of all the resistors is minimized by splitting each of the resistors into resistors of shorter length adjacently laid out and connected in series as shown in Figure 12(b). It can also be seen that the resistors are terminated on heavily doped P-type layers designated P^+ regions, to reduce the contact resistance between the resistor and the aluminum metal contact

Typically most commercial pressure sensors are operated at supply voltages V_{in} = 5 Volts. Assuming the typical values of π_1= 70 x 10^{-11} /Pa and ν=0.3 for a single crystal silicon, with a pressure sensor having a square diaphragm of $2a$ = 1000µm, h=25µm, the pressure sensor output voltage estimated using (17) is approximately equal to V_o = 117mV, when P=1.2bar = 1.2x10^5 N/m^2.(Note that 1N/m^2 =1 Pascal).

6. Performance Characteristics of Pressure Sensors

The main parameters and specifications of the pressure sensor are sensitivity in the linear range of operation, offset voltage, maximum V_0 in the linear range of operation, non-linearity for a specified maximum pressure of operation, the temperature coefficient of resistivity (TCR) and the temperature coefficient of sensitivity (TCS), hysteresis and creep. For the sake of clarity, the experimentally measured output characteristics of a pressure sensor having resistors fabricated on to

a polysilicon layer on oxide over a diaphragm is shown in Figure 13, to understand the various parameters and specifications. These output characteristics show a non zero output voltage, V_o, when the pressure is zero, followed by a linear V_o versus pressure region, and then a non-linear region beyond a certain pressure and are detailed below.

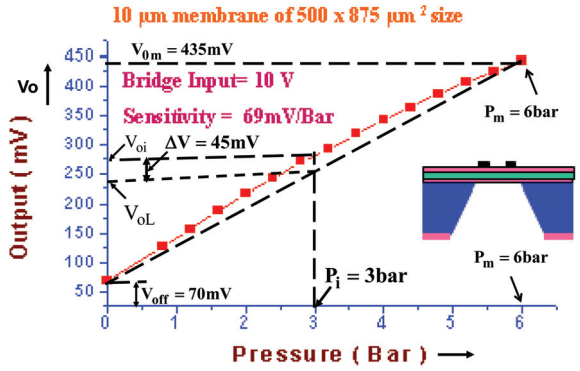

Fig. 13 Typical Output characteristics of a piezoresistive Pressure sensor, showing the Offset voltage and the nonlinear behavior beyond 2.0 bar

6.1 Offset Voltage

The output voltage of the pressure sensor at zero input pressure is designated as the offset voltage. This is due mainly to two reasons. The first one is due to some residual stress on the membrane. The second main reason is the variability in the four resistors. Even though the resistors are processed by diffusion simultaneously, there are some variations due to non-uniformity in the starting polysilicon layer or due to non-uniformity in dopant diffusion in the polysilicon resistor. Even a 5 Ω difference in the 1kΩ resistance values can cause an imbalance in the Wheatstone bridge and result in an output offset voltage of 50 mV for an input voltage of 10 Volt. Therefore, piezoresistive pressure sensors invariably show offset voltage. In Figure 13, this is marked and is equal to 70mV for an input voltage of 10V. One of the approaches used for offset voltage compensation has been to connect the external resistors. This involves the use of an open bridge configuration and the use of external precision resistors to complete the bridge during the packaging stage. Over the years, more elegant and efficient techniques of compensating for the offset voltage using electronics have evolved.

6.2 Sensitivity, S

The sensitivity of a pressure sensor is defined as $S = \frac{\Delta V_o}{\Delta P}$ at a particular input voltage. Considering the device characteristics shown in Figure13, the V_0 increases from 70mV to 210 mV linearly as the pressure is increased from 0 to 2.0bar. The sensitivity for this device is $S = \frac{210-70}{2}$ mV/bar and this is equal to 70mV /bar when the input voltage V_{IN} =10V The sensitivity is rather low for this device because the resistors in this case were fabricated using polycrystalline silicon whose gauge factor is low compared to that of single crystal diffused resistors. Higher sensitivities and lower noise levels are typically achieved with diffused or ion implanted single crystal silicon strain gauges.

6.3 Nonlinearity and the Ballooning Effect

Nonlinearity is a key parameter of pressure sensors and it is specified as a percentage of the full-scale output voltage of the sensor. Referring to the experimental characteristics shown in Figure 13, the full scale output voltage $V_{om} = 435mV$ at Pm = 6 bar and V_{off} = 70mV when P=0. The nonlinearity NL_i of this experimental pressure sensor at any intermediate pressure P_i is defined with reference to the end point straight line joining the point $V_o = V_{om}$ at P_m = 6 bar and at P= 0 by the following equation,

$$NL_i = \frac{V_{0i} - V_{0L}}{V_{0L} - V_{off}} \qquad (18)$$

In this expression, V_{oi} is the sensor output voltage at pressure P_i and V_{oL} is the value of V_o that would have occurred if the Output characteristics coincided with the end point straight line. It is given by the relation,

$$V_{oL} = V_{off} + \frac{V_{om} - V_{off}}{P_m} P_i \qquad (19)$$

It is seen from Figure 13 that at, P_i = 3bar, V_{oi} = 275 mV and V_{oL} = 230mV. The nonlinearity is $NL_i = \frac{45}{160} \times 100\% = 28.5\%$. However, when the Pm recommended for the same pressure sensor is

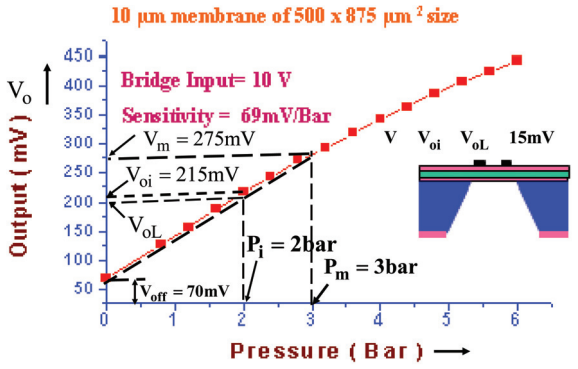

Fig. 14 Typical Output characteristics of a piezoresistive Pressure sensor, showing that the nonlinearity is lower if is chosen to be 3bar

changed to 3 bar, the corresponding V_m = 275mV and the end point line is as shown in Figure 14. The corresponding values of V_{oi} and V_{oL} are respectively 215mV and 205mV at a pressure P_i=2bar. Hence, the nonlinearity at P_i=2bar with respect to the corresponding to V_0 is considerably lower and is given by,

$$NL_i = \frac{V_{0i} - V_{0L}}{V_{0L} - V_{off}} \times 100\% = \frac{10}{135} 100\% = 7.5\%$$

Thus if the range of operation is restricted to the linear range the maximum nonlinearity within the operating range remains at an acceptable level.

Occasionally, one may encounter negative offset voltage. In such cases the above definition holds good and the sign should be appropriately taken into account. The nonlinearity in the piezoresitive pressure sensors is caused mainly by the following factors:

(i) The nonlinear relationship between the stress and the pressure applied. As discussed in section 3, if the deflection of the diaphragm is large compared to its thickness, the central plane of the diaphragm stretches like a balloon. Due to this balloon effect, the diaphragm is subjected to a stretching stress component, σ_s, in addition to the stress, σ_b caused by the bending of the diaphragm. The stress,σ_b, caused by bending, is reduced in magnitude as the stretch of the diaphragm takes part of the pressure load and this results in nonlinearity. The nonlinearity caused by the balloon effect (ie the stretch) is smaller when the sensor is subjected to pressure from the front side where the resistors are located. This is because σ_s is always positive irrespective of its position in the diaphragm and the direction of the applied pressure, whereas the polarity of σ_b can be either positive or negative depending on its position in the diaphragm and the sign of the applied pressure. Thus, both σ_s and σ_b are positive at the diaphragm edge when the pressure is applied from the front whereas σ_b is negative and σ_s is positive when the pressure is applied from the backside. Hence when the pressure is applied from the front side the stresses add up and the total stress tends to be closer to the linear theory which assumes that the stress distribution is a result of pure bending.

(ii) The piezoresistive coefficient of silicon is generally considered to be independent of stress. In practice, this is not really true when examined with high accuracy. The nonlinear relationship between the piezoresistive coefficient and the stress is thus another source of nonlinearity in piezoresitive pressure sensors.

(iii) The third cause of the nonlinear output voltage is due to the difference in piezoresistive sensitivity between the resistors of the Wheatstone bridge.

For low- pressure sensors, linearity becomes an issue. Bossed diaphragms or sculptured diaphragms, as will be discussed in subsequent sections, are used to overcome this problem.

6.4 Hysteresis

Hysteresis is yet another parameter of pressure sensors and this is also specified as a percentage of the full-scale output voltage of the sensor. This parameter is a matter of concern in pressure sensors, which employ metal diaphragms, because of the non-elastic characteristics of ductile metals, even with very good spring materials. However, single crystal silicon is an excellent spring material. At temperatures below 600°C, the silicon stress versus strain curve has no plastic zone and the material has essentially no creep. Pressure sensors employing a silicon diaphragm as a sensing element have hysteresis below 0.1%, which is very low.

6.5 Temperature Coefficients of Resistivity and Sensitivity (TCR and TCS)

Piezoresistivity is a consequence of the change in resistance due to a change in the mobility of

carriers due to pressure-induced strain. It is well known that resistivity is also a function of temperature due to a reduction in mobility at higher temperatures. The TCR is always positive in diffused single crystal resistors. The TCR of piezoresistors affects the sensitivity of the pressure sensor and leads to TCS which we show below to be always negative.

Consider the Wheatstone bridge circuit shown in Figure 12, which is balanced at room temperature and at zero pressure difference across the diaphragm. Due to the positive TCR, all the resistance values increase by ΔR_T when the temperature goes up by ΔT. This, alone, would not affect the output voltage because all the resistor values go up equally by ΔR_T. However, due to a change in the pressure, the P-type resistances R_1 and R_3 in Figure 12 increase by ΔR, and the resistance values R_2 and R_4 decrease by ΔR assuming them for simplicity to be the same in magnitude when pressurized from the backside of the diaphragm. The combined effect of pressure P and the temperature rise ΔT on the V_0 can be expressed as given below.

$$V_o = V_{in}\frac{(R+\Delta R+\Delta R_T)-(R-\Delta R+\Delta R_T)}{2R+2\Delta R_T} = V_{in}\frac{\Delta R}{R+\Delta R_T} \quad (20)$$

The temperature dependent term $\Delta Rt = R\alpha\,\Delta T$ where α is the TCR of the resistors R. Substituting this in equation (20),we have,

$$V_o = V_{in}\frac{\Delta R}{R(1+\Delta R_T/R)} = V_{in}\frac{\Delta R}{R(1+\alpha\,\Delta T)} \quad (21)$$

In this equation from (16) $\frac{\Delta R}{R} = \pi_t P \frac{a^2}{h^2}(1-\nu)$ and hence

$$V_o = V_{in}\pi_l P\frac{a^2}{h^2}(1-\nu)\frac{1}{(1+\alpha\,\Delta T)} \quad (22)$$

and the sensitivity can be expressed as

$$S = \frac{\Delta V_o}{\Delta P} = V_{in}\pi_l\frac{a^2}{h^2}(1-\nu)\frac{1}{1+\alpha\Delta T} = \frac{S_o}{1+\alpha\Delta T} \quad (23)$$

where S_o is the sensitivity when the temperature is constant. Generally, as $\alpha\Delta T << 1$, (23) can be written as,

$$S = S_o(1-\alpha\,\Delta T) \quad (24)$$

Equation (24) shows clearly that TCS in piezoresistive pressure sensors is reduced and that the extent of reduction in sensitivity depends upon TCR and the temperature change. In diffused single crystal resistors, TCR (=α) is always positive [Mosser et al., 1991] with its magnitude varying from 1×10^{-3} / °C to 2×10^{-3} /°C for doping concentrations in the range of 10^{18} / cm^3 and 10^{20} / cm^3. Assuming the value of α = 0.001/°C, when the temperature of the sensor goes up by 100°C, $\alpha\Delta T = 0.1$ then using this in (24), S= 0.9 S_0 indicating a 10% fall in sensitivity.

The TCS can cause severe errors in the pressure being monitored. The magnitude of the error will be severe when ΔR_T is comparable to the change in the resistivity ΔR caused by the pressure. Commercial ASIC chips are used to compensate for the TCS and the offset voltage. Another approach to minimize this effect is to use polycrystalline silicon (poly-Si) piezoresistors with the TCR tailored suitably by altering the doping concentration [Mosser et al., 1991].

7. Polycrystalline Piezoresistive Pressure Sensors

In conventional single crystal silicon piezoresistive pressure sensors, the four P-type piezoresistors constituting the Wheatstone bridge are embedded on an N-type silicon diaphragm either by ion implantation or a diffusion of boron process. Thus the resistors are isolated from each other on the diaphragm by PN junctions which can be effective only till about 100 °C. Yet another issue with this approach is that the resistors need to be isolated from the header on which the device is mounted either by anodic bonding glass to silicon or by Fusion bonding an oxidized silicon wafer. The above problems can be sorted out by realizing the resistors on an oxide layer grown on a Silicon On Insulator (SOI) wafer.

7.1 Polycrystalline Piezoressitive Pressure Sensor On SOI Wafer

In this approach the SOI layer itself serves as the diaphragm, with the handle wafer etched using anisotropic etching from the backside. P-type polycrystalline silicon resistors are realized on the oxide grown on the SOI layer as shown in Figure

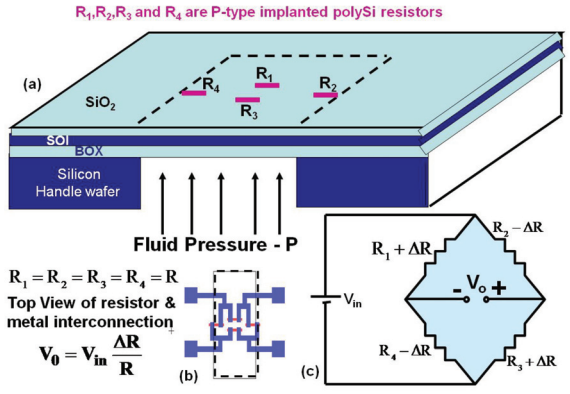

Fig. 15 Polysilicon pizoresistive pressure sensor on oxidized SOI diaphragm

15 (a), by depositing, doping and patterning the polysilicon. The deposition of polysilicon is carried out by a low pressure chemical vapor deposition (LPCVD) process, and the P-type doping is achieved by the ion implantation of boron followed by annealing. With this approach, P-type polysilicon resistors are isolated from each other by the oxide layer. Therefore, the isolation between the resistors is maintained even at temperatures in excess of 300 °C. The pressure sensor fabrication is completed at the wafer level by depositing and patterning chrome /gold or Al as shown in the top view in Figure 15(b) to connect them in the form of the Wheatstone bridge shown in Figure 15(c).

7.1.1 Resistivity and TCR

The resistance of grains and that of grain boundaries determine the effective resistance of polysilicon resistors, the latter being the most important aspect. Within the grains, the current transport is by carrier drift, and the resistivity of the grain region behaves essentially like that of the single-crystal silicon resistor. Therefore, it increases with temperature due to a reduction in mobility. On the other hand, the grain boundaries offer potential barriers for carrier transport across them. At higher temperatures, more carriers gain energy sufficient to cross over these barriers, and the grain boundary resistance decreases with temperature rise. The barrier height at the grain boundary is a function of doping concentration. Therefore, the temperature coefficient of resistivity (TCR) of polysilicon can be tailored and made almost zero by adjusting the boron doping concentration [Mosser et al., 1991] so that the positive TCR of the grains can be balanced by the negative TCR of the grain boundary regions. The experimental results reported recently [Raman et al., 2006; Manjula, 2005] on boron-implanted LPCVD polysilicon films of thickness 0.3μm are presented in Figure 16 to show that the TCR of LPCVD polysilicon resistors can be negative, approach zero, or be positive depending on the doping density. It can be seen that the TCR can be reduced to a low value equal to 1.75×10^{-5}/°K with the room temperature resistivity, $\rho = 1.05 \times 10^{-2}$ Ω - cm for doping concentration $N_A = 2.66 \times 10^{19}$ / cm^3.

7.1.2 Alternate Layout on a Rectangular Diaphragm

The multiple orientation of the crystalline silicon in the grain makes an average contribution in all possible directions to the piezoresistance of the polysilicon film. Therefore the piezoresistive effect in polysilicon film is isotropic [Xiaowei et al., 1998] and is less than in single crystal silicon. The magnitude of the longitudinal gauge factor (G_L=30) of boron-implanted polysilicon is larger than the transverse gauge factor (G_T = -10) [Mosser et al., 1991] by a factor of about 3. Polysilicon piezoresistors therefore are arranged n the diaphragm in such a way that they experience maximum longitudinal stress in order to achieve better sensitivity. The results of a study presented in Figure 6 in section 3 show that the x-component of the stress is a compressive maximum at x=±*a*,y=0 and it is a tensile maximum at x=0, y=0 when the pressure is applied as shown in Fig.15. The simulation results presented in Figure 8 and 9 also demonstrate that the magnitude of these stresses are maximum when the diaphragm is rectangular with an aspect ratio *b/a* = 2. The rectangular diaphragm is deliberately chosen and the resistors are placed as shown in Figure 15(b) along the narrower direction and connected in the Wheatstone bridge as in Figure 15(c) to achieve a maximum possible sensitivity.

Several possible arrangement patterns of polysilicon resistors have been studied for different geometrical sizes of the membrane and the results [Xiaowei et al., 1998] have shown the following: (1) The arrangement Pattern shown in Figure 15(b) gives the best results in terms of maximizing the

output voltage of the sensor because, the piezoresistors take advantage of the longitudinal piezoresistive effect of polysilicon and placed along the narrower direction. (2) In the sensor design, the length to width ratio of the rectangular membrane should be increased to some degree to enhance the output.

7.1.3 Experimental Results

Based on these studies, boron implanted and annealed LPCVD polysilicon resistors are arranged on the oxide grown on a silicon diaphragm as shown in Figure 15(b) and connected in a Wheatstone bridge configuration as shown in Figure 15(c) on an oxidized rectangular diaphragm of thickness 15µm and a lateral dimension equal to500µm x 875 µm. The individual devices were diced and mounted on the TO-5 header, wire bonding was carried out and a cap with a pressure port was welded. Figure 17 shows the photograph of the packaged device with the pressure port. The figure also shows the close-up photograph of the chip, four wires bonded on to the pads and the photograph of the chip mounted inside the package on the header [Bhat et al., 2006]. The output voltage Vo as a function of pressure in the range P=0 to 15bar of these packaged devices is obtained for two different applied input voltages V_{in}=1V and V_{in} =2V. The typical results obtained are shown in Figure 18. It can be seen that the characteristics are linear over the entire range of pressure upto 15 bar. As the gauge factor of polysilicon is rather low, and also because the diaphragm was designed with a thickness of 15 µm for operation up to 15bar pressure with burst pressure in excess of 100bar, the sensitivity in these devices were found to be in the range of 1.8mV per bar forV_{in} = 1.0 Volt. The temperature sensitivity of these devices was tested in the temperature range 30°C to 70°C and the results [Bhat et al., 2006] are shown in Figure 19. The variation in sensitivity was found to be within about 5% of the room temperature value. Similar results are seen in Figure 19 on another sensor with a diaphragm thickness of 10µm. The sensitivity of this sensor is much higher (6mV/bar) as expected because of the lower thickness. As a result, the temperature sensitivity of these devices was found to be slightly lower than 3% because the TCR term ΔRT is invariant with the diaphragm thickness

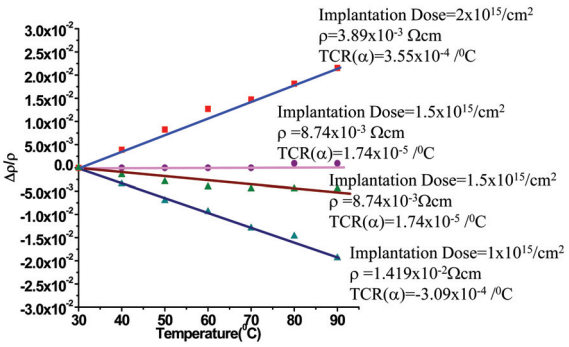

Fig. 16 Experimental results on the effect of boron doping concentration on the TCR of polysilicon resistors [Manjula, 2005].

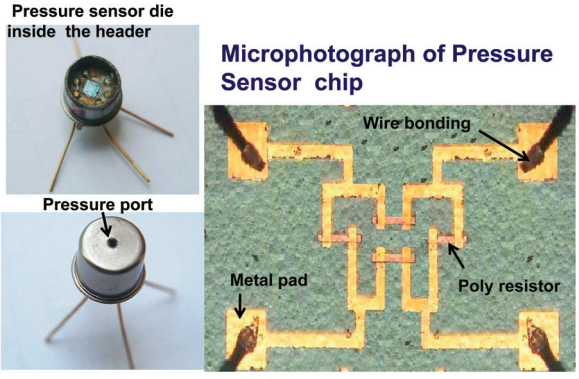

Fig. 17 Photographs of polysilicon Pressure sensor inside the TO-5 Package and a close up view of the wire boned chip.

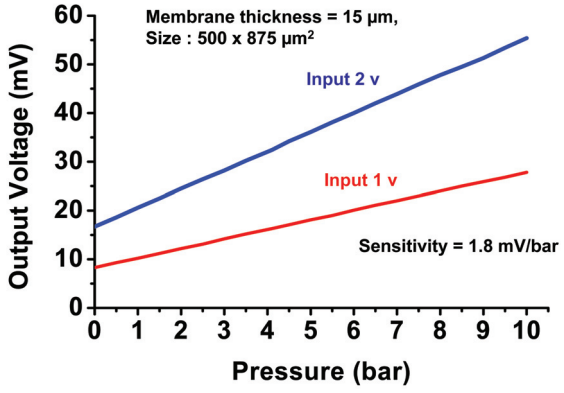

Fig. 18 Output voltage versus the input pressure measured on the pressure sensor shown in Fig 17.

whereas the pressure dependent term ΔR is higher with the thinner diaphragm.

These results have indeed demonstrated that the TCS of piezoresistive polysilicon pressure sensors can be minimized by suitably doping

LPCVD polysilicon resistors such that the TCR is below 10^{-4}/C. The SOI approach for realizing the diaphragm, not only provides the high isolation required between the sensor and the body of the package, it also makes it easy to achieve a diaphragm of uniform thickness over the entire wafer, thus enhancing the reliability and reproducibility of the pressure sensors.

7.2 SOI Approach for Monolithic Integration

The ultimate success of silicon micromachining in smart systems depends upon the ability to integrate mechanical components with electronics on the same chip. The possibility of the monolithic integration of piezoresistive pressure sensors with electronics has been demonstrated at the Indian Institute of Technology Madras [Vinoth Kumar et al., 2006; Vinoth Kumar, 2006]. Figure 20 (a) shows the schematic cross section of the MOS Integrated piezoresitive pressure sensor designed and fabricated on a single chip. In this approach, the starting wafer was an SOI wafer and polycrystalline silicon resistors deposited on oxide were used for achieving better electrical isolation between them as well as between the electronics circuit and the sensor. The sensor output is connected to the input of a common source differential amplifier circuit

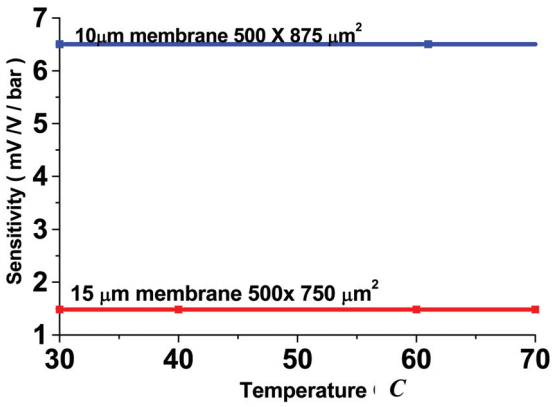

Fig. 19 Temperature sensitivity of two different Poly Silicon piezoresistive pressure sensors having the diaphragm dimensions indicated on the plots [Bhat et al., 2006]

as shown in Figure 20(b). The resistors are embedded over the diaphragm, which is realized by anisotropic etching, and the electronics circuit is laid out in the rest of the portion on the same chip as shown in Figure 20(a). Integration with fewer process steps has indeed been possible by merging the process steps of polysilicon piezoresistors with the resistors of a common source differential amplifier circuit. The self-aligned polysilicon gate MOSFET technology was used for the electronics circuit in this chip. The MOSFET integrated

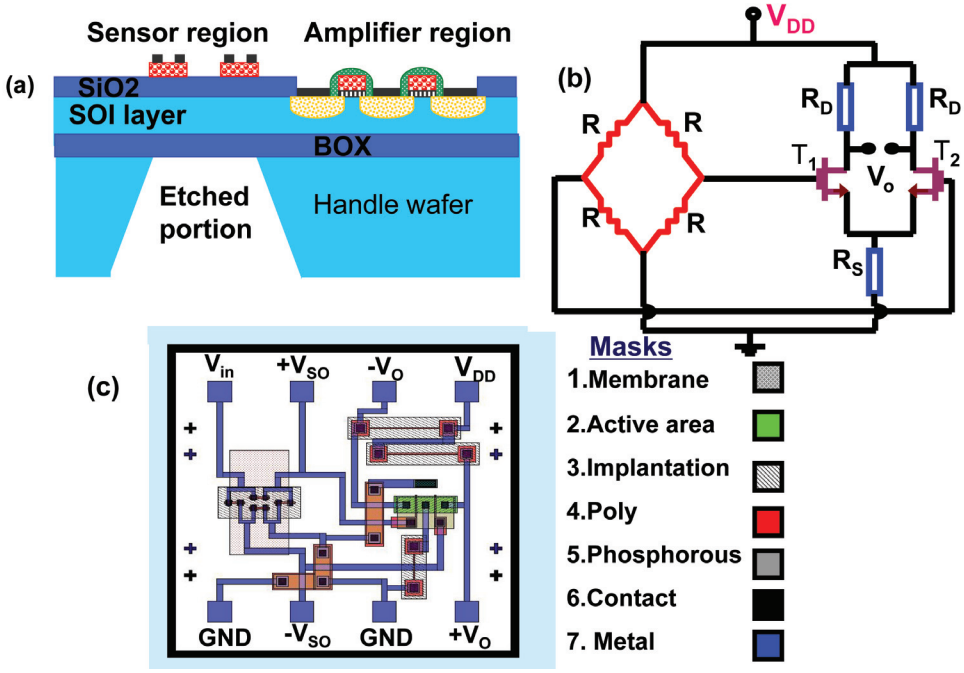

Fig. 20 (a) Schematic Cross section (b) Sensor and the amplifier circuit and (c) Composite mask layout of the MOS Integrated pressure sensor. Chip mounted on header and wire bonded (e) Packaged sensor showing the pressure port.

piezoresistive pressure sensor is fabricated using a seven-mask process. A composite layout of the seven masks is shown in Figure 20(c). In this layout, provision is made for accessing the sensor output as shown by the pads marked $+V_{SO}$ and $-V_{SO}$ which are connected to the MOSFET gate electrodes. The supply voltage terminals are marked $+V_{DD}$ and $-V_{DD}$ and the output of the amplifier is labelled as V_O.

The photographs of the integrated chip, the chip die mounted on the TO-39 header and wire bonded, and the final package are shown in Figures 21 (a), (b) and (c) respectively. The sensor output voltage V_{SO} and the amplified output voltage V_O measured in the pressure range of 0 to 7 bar are presented in Figure 21(d). The on-chip amplifier gain was designed to be about 5. The overall sensitivity of 270 mV /bar with 10V supply voltage has been achieved with this MOS integrated piezoresistive pressure sensor.

At this stage, it is to be noted that the above exercise of packaging was meant for testing the integrated sensor at the laboratory. However as will be seen in the subsequent section on Packaging, several requirements need to be met by the packages operation in harsh environments and they need to be tailor made to suit specific applications.

8. Low -Pressure Sensors with Sculptured Diaphragm

As the maximum stress in a flat diaphragm with lateral dimensions of $2a$ and thickness is proportional to $P(a/h)^2$, the sensitivity of a piezoresistive pressure sensor fabricated on a flat diaphragm can be increased by making the (a/h) ratio larger. However, it can be seen from equation (2) that the deflection w_o to thicknessb h ratio is proportional to $P\ (a/h)^4$. Therefore, in a low

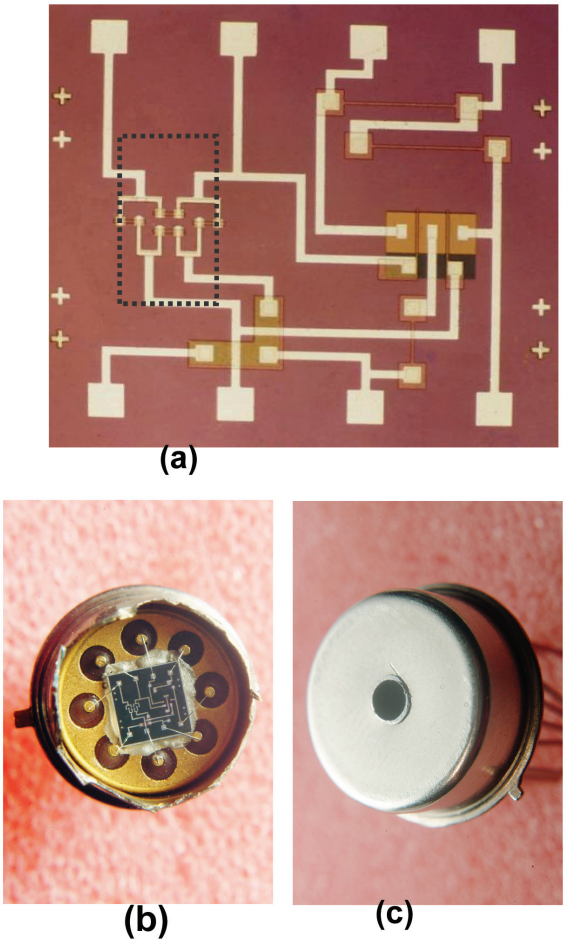

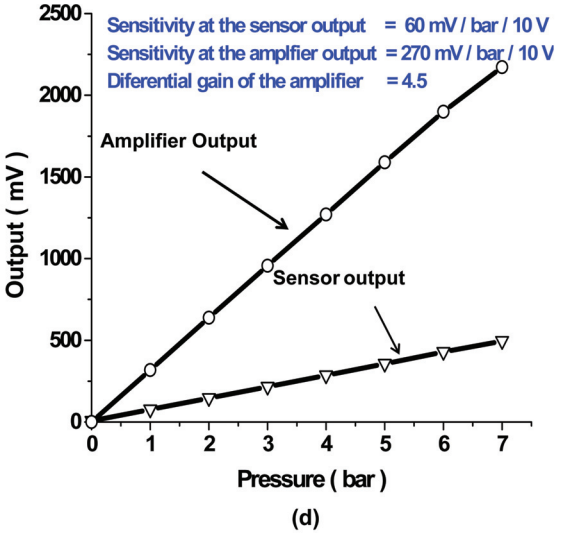

Fig. 21 Photographs of (a) MOS integrated Pressure sensor chip (b) die mounted on the TO-39 header and wire bonded (c) Packaged sensor showing the pressure port. (d) Output Characteristics versus pressure.

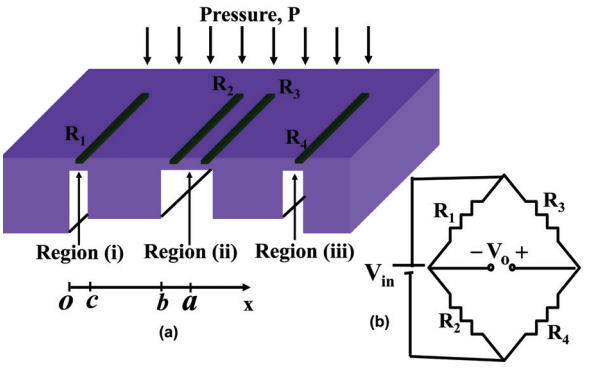

Fig. 22 (a) Pressure sensor with sculptured diaphragm (b) Wheatstone bridge connection of the resistors (note that R1 and R4 are on opposite arms and R2 and R3 are on the other opposite arms of the bridge

pressure range (e.g. a full-scale pressure of about 500Pa), flat-diaphragm pressure sensors are not suitable because the sensitivity will have to be increased considerably by making the (*a*/*h*) ratio extremely large and this would lead to large deflections resulting in a high degree of nonlinearity. As discussed before, non-linearity is the result of the stretching of the middle plane, which becomes significant when the deflection becomes comparable to the thickness of the diaphragm. In order to improve sensitivity and linearity simultaneously, specialized geometries, such as diaphragms with a rigid center or boss [Mallon et al., 1990] have been introduced for increasing the stiffness to limit the maximum deflection of the diaphragm, and for enhancing linearity. Such a structure is also known as the sculptured diaphragm or the bossed diaphragm and is schematically shown in Figure 22 [Mallon et al., 1990]. In this approach, the structure is locally stiffened to limit the overall deflection, while maintaining a relatively thin section where the piezoresistors are placed. Thus the total nonlinear deflection due to membrane stress is reduced. Since the deflection and resulting stress occur at a localized area, and also because the stress is concentrated in relatively localized thin areas of the diaphragm, this technique is sometimes referred to as the stress concentration technique. This term is rather misleading because the stress at the edge of a flat diaphragm of thickness h is found to be higher than the stress on the same diaphragm with a central double boss structure. However, the linearity of deflection with pressure improves considerably with the bossed structure. Thus, in summary, the sculptured diaphragm structure provides lower deflection and better linearity at a given stress level but does not enhance the stress by concentrating it in a small area.

As can be seen from Figure 23 (a), in a double bossed diaphragm, all the four resistors are subjected to transverse stress when the structure is subjected to pressure. When pressure P is applied to it from the top surface as shown, resistors R_1 and R_4 which are laid on the thin regions (i) and (iii) of thickness, h, experience identical transverse tensile stress and are connected to the opposite arms of a Wheatstone bridge as shown in Figure 23(b). On the other hand, resistors R_2 and R_3 which are laid on the thin region (ii) of thickness, h, experience transverse compressive stress and are connected to the other opposite arms of the Wheatstone bridge. A detailed analysis [Bao, 2000] of this structure has shown that the average transverse tensile stress on resistors R_1 and R_4 placed in the regions-(i) and (iii), is=1.35 $P(a/h)^2$ and the average transverse stress on resistors R_2 and R_3 placed in the region-(ii) is=-1.35 $P(a/h)^2$, the negative sign indicating that the stress in this case is compressive. It has also been shown in [Bao, 2000] that the output voltage from the pressure sensor and the maximum deflection w_o can be approximated in terms of the thickness h of the thin region where the resistors are placed on the twin –bossed diaphragm and the lateral dimension, a, shown in the Figure 23, by the following expressions

$$V_o = 0.75P\frac{a^2}{h^2}(1-\nu)\,\pi_t V_{in} \qquad (25)$$

$$\frac{w_o}{h} = \frac{Pa^4}{2Eh^4 g_1}$$

where $$g_1 = \frac{4.13}{1-\nu^2} = 4.54, \qquad (26)$$

Comparing v_o in eqn (25) with the expression v_o in eqn (17) for the flat diaphragm, it can be seen that the sensitivity of the twin island structure sensor is lower by a factor of 0.75 compared to the sensitivity of a flat diaphragm of uniform thickness h and the same side length equal to $2a$. Similarly, comparing equation (26) with equation (2), it is evident that the w_o/h ratio in this twin island structure is lower by a factor of 2 than in the flat

membrane situation, thus illustrating that linearity can be maintained at higher pressures for a given thickness. Alternatively a thinner diaphragm can be used for better sensitivity and for maintaining better linearity compared to a sensor with a flat diaphragm.

In summary, piezoresistive pressure sensors using the sculptured structure give better linearity and, hence, are used as a widely accepted technique for sorting out the difficulties faced when used with flat diaphragm sensors for applications in sensing very low pressures.

An alternative solution for very low pressures is the **capacitive sensing approach.** However, there are several problems associated with capacitive sensing: (1) The stray capacitance needs to be minimized and compensated for (2) Capacitance to voltage conversion is a must (3) Fabrication of capacitive pressure sensors is more involved than the piezoresistive counterpart. (4) Capacitive sensors are more susceptible to Electro Magnetic Interference (EMI) effect. Consequently, many commercial pressure sensors are piezoresistive.

Recently, **resonant sensors** have attracted considerable attention because of their ability to provide high resolution, high stability and an easy interface with digital circuits. Therefore, during the past two decades, efforts have been directed towards realizing resonant pressure sensors. In this approach, the change in the resonance frequency of a resonating structure caused by mechanical stress is monitored. Even though a few of them have been commercialized, their use in commercial products has been slow because of the complexity in processing and the need for packaging them in a vacuum to maintain high quality factor Q. A Digi Quartz resonating beam pressure sensor is being used as a bottom pressure recorder (BPR) for tsunami sensing applications.

9. Silicon Carbide Pressure Sensors for Harsh Environments

9.1 Silicon Carbide Piezoresistive Pressure Sensors

The applications of conventional piezoresistive silicon pressure sensors are limited to below 150°C due to the degradation of the PN junction isolation between the resistors on the diaphragm. Silicon On Insulator, along with oxide isolated piezoresistive elements, has enabled their use up to about 300°C. However, the need for pressure measurements in high-temperature (>600°C) and harsh environments (automotive and aerospace applications: combustion processes or gas turbine control; oil industry; industrial process control; nuclear power) has spurred the development of robust, reliable pressure sensors. This is mainly because of the poor thermo-mechanical properties of silicon, *viz* the degradation of the elastic modulus above 600°C, and its inability to withstand a corrosive environment. As a result, during the past decade, considerable effort has been directed towards taking advantage of the superior thermo mechanical properties of silicon carbide (SiC) to develop micro-pressure sensors that would extend the sensing capability to 600°C and beyond. The wide band gap of 3.3eV 6H-SiC enables high temperature operation of the junctions. The fairly inert nature of the SiC makes it suitable for use in corrosive environments, and the electronic circuits on SiC are radiation-insensitive. As already presented in Table-1, the gauge factor of single crystal SiC is in the range 10 to 30 and in polycrystalline SiC, it is in the range of 3 to 5. The properties of Single crystal SiC are presented in Table-3, and are compared with Silicon and diamond to show that the yield strength , Young's modulus and hardness of SiC are considerably higher than those of Silicon and are closer to those of diamond.

In spite of its several merits, the development of SiC pressure sensors has been slow because of the difficulties involved in its micromachining. Initially, SiC piezoresistors were fabricated on oxide grown on a silicon micromachined diaphragm. In this approach, silicon becomes the limiting factor. The benefits of SiC material can be fully utilized by fabricating both the piezoresistive sensing elements and the sensing diaphragm on SiC. This has, indeed, been made possible, as reported in [Ned et al., 2004], by micromachining N-type SiC in the DRIE system in a gas plasma mixture containing SF_6 and Oxygen to realize the SiC diaphragm. SiC piezoresistors were realized on the SiC diaphragm by chemical vapor deposition of SiC using a gas mixture of SiH_4 and CH_4 and patterning it by RIE. Ohmic contacts on the SiC resistors were obtained with a Ti/Al bi-layer having 125nm titanium thickness and 1200nm of Aluminum. Both low and high

Table-3 Some important properties of single crystal Si, SiC and diamond [Peterson, 1982]

Property	Yield strength (GPa)	Hardness (Kg/mm^2)	Young's modulus (GPa)	Melting point (°C)	Gauge factor
Si	7	850	190	1410	100-200
6H-SiC	21	2480	700	2830 (sublimes)	10-30
Diamond	53	7000	1035	4000 (Phase change)	—-

pressure SiC piezoresistive pressure sensors operational up to 600°C have been demonstrated [Ned et al., 2004], using relatively thick (60 μm) diaphragms for the 1000 psi sensors, while the diaphragm for the 25 psi pressure sensor was micromachined to be significantly thinner with optimized sculptured sensing diaphragms of the type discussed in section-8. Although the performance characteristics such as sensitivity, linearity and hysteresis were reasonably good, a couple of issues still needed to be sorted out (1) A large thermal set (10mv) was observed in all SiC sensors after exposure to 600°C. (2) The bridge resistance versus temperature showed a non-monotonic resistance change with temperature, giving rise to a monotonic reduction in resistance up to 350 °C followed by an increase in resistance. This continues to pose a big challenge for the temperature compensation of such SiC sensors.

An exploratory effort [Vandelli, 2008] has shown that capacitive SiC MEMS devices fabricated and characterized showed a repeatable hysteresis less than 2.5% at 300°C. It was also demonstrated that the combined effect of temperature and pressure on non-linearity and hysteresis was never much higher than 1% FSO over an operating temperature range of 0 to 200°C.

According to a SiC road map [Fraga et al., 2010], the development of SiC sensors is based on progress in (1) the improved electrical and mechanical properties of SiC films produced by the optimization of the SiC deposition process, (2) SiC film processing by the optimization of the etching process and metallization appropriate for high temperature applications, (3) micro-fabrication technology to fabricate miniaturized sensors and (4) sensor packaging for harsh environments. The immediate goal is to improve the performance of SiC pressure sensors and strain gauges by optimizing all the four technologies above.

9.2 SiC -Capacitive Pressure Sensors for High Temperatures > 500°C

Capacitive pressure sensors are attractive for high-temperature applications because their performance is almost independent of temperature, and high sensitivity can be achieved with a low turn-on temperature drift. These devices are also less sensitive to side stress and environment variations. Capacitive sensors are best suited for low pressure and high temperature sensing applications ranging from low temperatures up to 500 °C and beyond with SiC diaphragms. A schematic structure of one such device [Du et al., 2003] fabricated with a 0.5 ìm single crystal 3C-SiC diaphragm on a single crystal <100> silicon is shown in Figure 23. A thin layer of phosphorous silicate glass (PSG) on the surface of the DRIE-etched silicon substrate provides electrical isolation between the SiC diaphragm and the DRIE-etched silicon substrate. When the diaphragm is subjected to pressure, P as shown in Figure 23(a), the capacitance increases nonlinearly due to its downward deflection till it touches the substrate at a designed touch pressure point (TPP). At this pressure, the diaphragm touches only at its middle. Beyond the TPP, the touching area increases and the capacitance increases linearly as shown in Figure 23(b). With the capacitance structure having a circular SiC diaphragm of 400μm, thickness 0.5 μm suspended over a 2 μm cavity in the silicon substrate, high sensing capability up to 400 °C has been reported in the literature [Du et al., 2003] with excellent linear characteristics in the pressure range between 1100 Torr and 1760 Torr with a sensitivity of 7.7fF/Torr.

These results have indeed demonstrated the benefits of using SiC diaphragms for high temperature operations and a capacitive sensing approach for low-pressure operations and this has opened up new avenues for future work for sensors using SiC. The development of high temperature

SiC electronics with SiC pressure sensors and SiC temperature sensors for intelligent engine systems is being pursued in academic institutions and industries. Semiconductor integrated circuit chips capable of giving over 100-fold improvement at 500 °C operational durability have been reported using Silicon Carbide transistors and logic circuits [Mohamed et al., 2010]

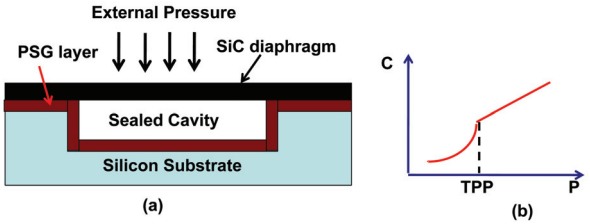

Fig. 23 SiC capacitive Pressure Sensor (a) the schematic structure (b) typical Capacitance, C, versus Pressure, P, characteristics showing the Touch Point Pressure (TPP)

10. Carbon Nano Tube (CNT) Based Sensors

In recent years CNTs-based pressure sensors have drawn considerable attention due to their high sensitivity, small size, low power consumption, and strong mechanical stability, in addition to thermal stability. The CNT-based pressure sensor can be operated up to 250 °C as against the 125°C of conventional PN junction-isolated silicon pressure sensors. The high gauge factors of about 1000 and the small size(diameter 1 to 100nm) of CNTs make them ideal for miniaturized pressure sensors for biomedical applications as well. The piezoresistive effect in the aligned multi-walled carbon nanotube (CNT) array arises due to the buckling of individual carbon nanotubes when compressed, leading to a decrease in the electrical resistance of the CNT array. Recently, it has been experimentally proved by mechanical loading of the array that the decrease in resistance is almost fully recoverable once the load is removed [Mohamed et al., 2010]. In the same paper, it has been shown that the change in the resistance increases linearly when 100 g and 500 g load are applied at a temperature of 20°C to 180°C, thus demonstrating that the multi-walled carbon nanotube (MWCNT) array is an excellent pressure and strain sensing element capable of operation at elevated temperatures.

A novel polymer-based MEMS pressure sensor has been reported [Fung et al., 2005] using bulk MWNT as the piezoresistive sensing elements. The development of the pressure sensor includes the fabrication of 300 thick Polymethylmethacrylate (PMMA) diaphragms using an SU8 molding/hot-embossing technique and AC electrophoretic manipulation of MWNT bundles on the diaphragms. The advantage of MWNT bundles is the ease with which they can be formed across electrodes on top of pressure diaphragms to serve as sensing elements. A schematic structure of the pressure sensor reported in [Wong et al., 2000] is shown in Figure 24. It has been shown that the diaphragm deflects due to an applied pressure and the MWNT piezoresistor gets strained, as a result, causing a change of resistance of 4 kW at a pressure of 70kPa from an initial value of 153kW at zero pressure. The CNT, as a sensing element on diaphragms using various materials is of great interest, and considerable effort has been expended over the past decade with varied degrees of success.

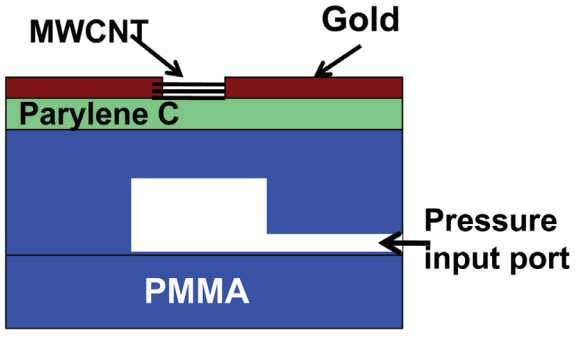

Fig. 24 Schematic diagram of MWCNT based pressure sensor reported in [Mohamed et al., 2010]

11. High Pressure Piezoresitve Silicon Pressure Sensors

We present the details of achievements on a high pressure sensor project taken up recently in the Centre for Nano Science and Engineering at the Indian Institute of Science Bangalore, as part of the National Program on Micro And Smart Systems (NPMASS) directed by Dr V.K. Aatre, former Scientific Advisor to the Defense Minister.

11.1 Design Considerations

In this section, we present the design considerations and wafer level processing approach required for high pressure piezoresistive pressure sensors capable of operation in the pressure ranges 100 bar to 400 bar (40MPa). They are presented along with packaging challenges and techniques for

meeting the specifications after integrating with an ASIC chip in the same package for offset and temperature compensation.

As discussed in section 5, the pressure sensor chip design involves the mask layout based on detailed simulation/analytical studies to determine both the diaphragm dimensions and the resistor locations and dimensions. The lateral dimensions of the sensor are chosen to provide enough width for placing the resistors. Additional requirements such as the chip size of the pressure sensor enforce further constraints on the maximum size of the diaphragm. In most situations, the diaphragms are square with a side length $L\,(=2a) = 500$ to 1000μm. Thus, when the diaphragm thickness h is in the range 10 to 50μm and is anchored at the bottom as shown in Figure 12(a), the theory of plates holds good. Hence, when the diaphragm is subjected to pressure, the maximum stress occurs in the middle of the diaphragm edges. Threfore, the resistors are embedded at the diaphragm edges as shown in Figure 12(b). However in sculptured diaphragms having bossed structures, and in high pressure sensors having very thick diaphragms, the diaphragm width L may turn out to be comparable to the thickness, h. In such situations, the simple theory of plates cannot be applied to determine the location of maximum stress.

Recent simulation studies [Thyagarajan & Bhat, 2013] conducted using the FEM tool COMSOL on micromachined diaphragms with the diaphragm anchored as shown in Figure 12(a) and Figure 15 have revealed that the location of the peak longitudinal stress on the top surface of the chip depends upon the L/h ratio of the square diaphragm side length $L\,(=2a)$ and thickness h. The exact location of the peak stress component is also found to depend on whether the diaphragm is carved out by the wet chemical or dry etching process. Wet chemical anisotropic etching such as KOH etching results in the cavity having side walls slanting at an angle of 54.74° to the diaphragm, as shown in Figure 12(a). On the other hand the sidewalls of a cavity etched by deep reactive ion etching (DRIE) are perpendicular to the diaphragm, as shown in Figure 15, making the transition from the diaphragm abrupt. As a result the stress distributions in the two cases are different. Figure 25 shows the simulation results obtained on the location X_p of the peak of the stress component along the width of the diaphragm on the top surface, for different L/h ratios, considering a few typical thicknesses. It is clearly seen from this result that the location of the peak stress lies outside the diaphragm portion when the L/h ratio is below a certain minimum value which is determined by the cavity geometry (slanted or vertical) and the diaphragm thickness. The simulation results on the stress distribution [Thyagarajan & Bhat, 2013] across the diaphragm surface are shown in Figure 26 for a specific thickness of the diaphragm when the L/h ratio is 3.75, for different applied pressures ranging from 10bar to 100bar. Here the location of the peak stress lies outside the diaphragm region and that the location is independent of the magnitude of the pressure. The peak value of this stress varies linearly with pressure, suggesting that P-type piezo-resistors can be embedded around this region orienting them either perpendicular or parallel to the diaphragm edge which is in the <110> direction.

11.2 Fabrication, Characterization and Results

The thickness, h, and lateral dimensions, L of the diaphragm are chosen based on the maximum pressure of operation, while ensuring that the burst pressure is at least five times that of the maximum pressure of operation. The resistors are embedded inside, outside or partly inside the diaphragm, depending upon its L/h ratio. An image of the 400bar pressure piezoresistive pressure sensor chip fabricated in the National Nano Fab of the Centre for Nano Science and Engineering (CeNSE) at the Indian Institute of Science, using the above design criteria is shown in Figure 27(a). Here, each resistor is split into two portions to accommodate them within the high stress region, and are connected in series using a P^+ diffused region. The resistors were fabricated by the boron diffusion process, which was standardized to achieve a sheet resistivity of 150-200 Ohms/square in the initial trial runs. Ion implantation was carried out at Bharat Electronics (BEL), Bangalore to achieve precise sheet resistance in the final process runs. The chip size is 2mm x 2mm, and the diaphragm is realized using DRIE. Aluminum metal was sputtered and patterned to realize the Wheatstone bridge of the transducer. Initially, the devices were tested at the wafer level by probing them to ascertain the functionality of the sensor and to determine the

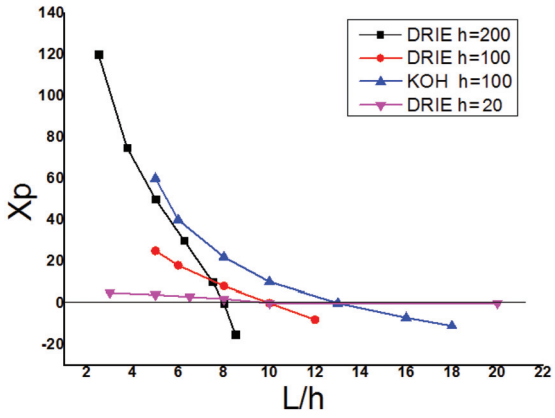

Fig. 25 Location *Xp* of peak stress with respect to the diaphragm edge for different diaphragm for KOH and DRIE cases as a function of the aspect ratio *L/h* for typical values of diaphragm thicknesses.

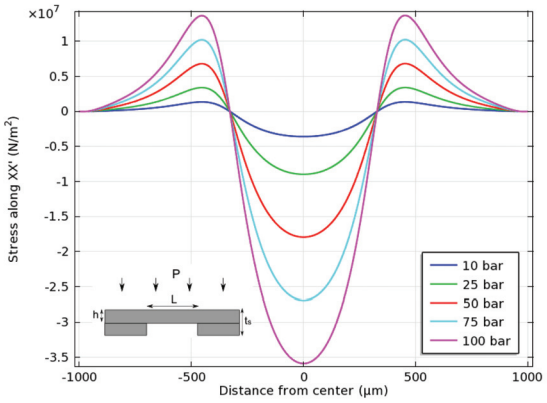

Fig. 26 Stress distribution on the top surface of the diaphragm along the width of the diaphragm for different magnitudes of pressure *P* (in bars) = 10, 25, 50, 75, and 100 applied on a thick DRIE diaphragm having *L/h* <7

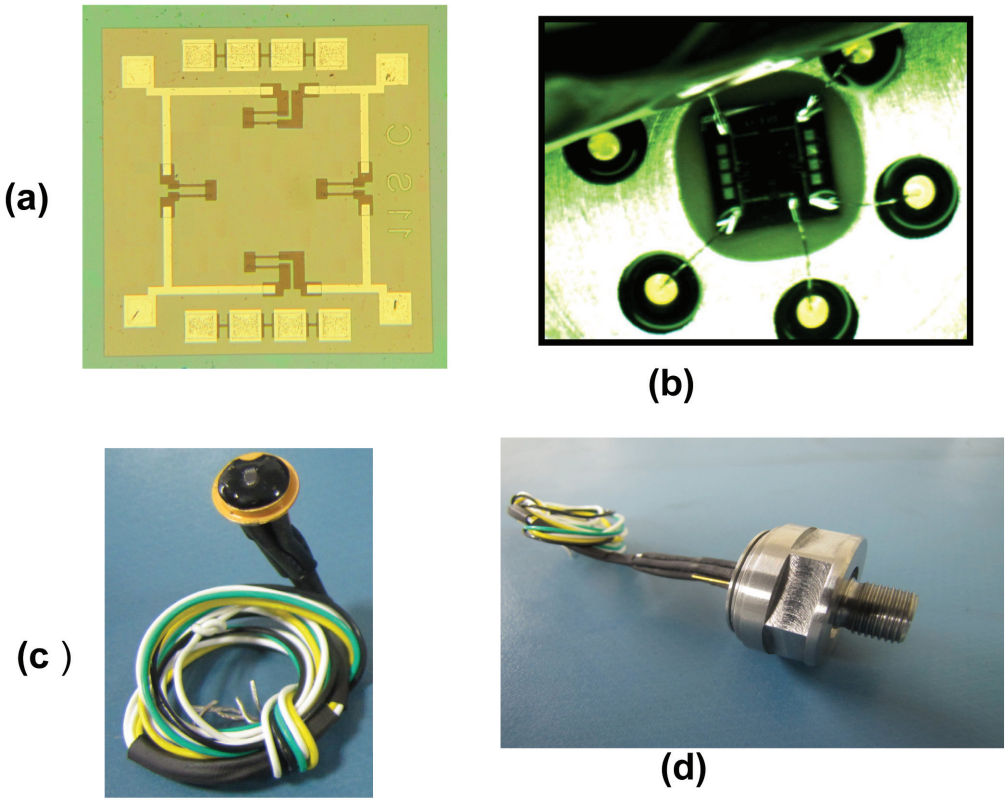

Fig. 27 Photographs of a 400bar piezoresistive pressure sensor fabricated at CeNSE, showing (a) the chip (b) chip mounted on header and wire bonded (c) wire connected to the electrical port of the package showing the chip in position (d) completed package with pressure port and electrical connection.

offset voltage. The devices diced from the wafer were die mounted on headers, wire bonded and packaged with oil filling along with a stainless steel second diaphragm and tested up to 400 bar. A photograph of the chip mounted on the header and wire bonded on to the pads is shown in Figure 27(b). External wire connections were made to the device and brought out of the header as shown in the photograph 27(c). The packaging was completed by appropriately welding the pressure port. A photograph of the completed device is shown in Figure 27(d).

Another set of devices was packaged at BEL with oil filling and sealing as required by a commercial application. They were tested at CeNSE. The typical output characteristics measured on the packaged 400bar sensor are presented in Figure 28. A full scale output of 116mV at 400bar is achieved on the packaged sensor with a sensitivity of 29mV/100bar. Excellent sensitivity and linearity within 0.2% with respect to the full scale output (FSO) of 400bar pressure was achieved. As can be seen, the hysteresis is insignificant.

Packaging these high-pressure sensors is quite different and more complicated than the TO-39 packages presented in section 7. The details of the technology and the challenges involved in packaging these high pressure sensors for operation in harsh environments, and for absolute pressure , gauge pressure and differential pressure sensing, are presented in the following section.

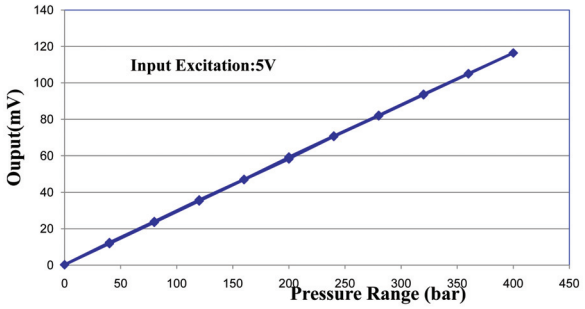

Fig. 28 output characteristics of the 400bar pressure sensor

12. Packaging Technology

The requirements and constraints imposed on MEMS pressure sensor/transducer packages are briefly presented here. The associated challenges and techniques used for realizing microsystem packages are presented with examples drawn from various types (Absolute, Gauge or Relative and Differential) of pressure sensors.

12.1 Introduction

Micromachined (MEMS) pressure sensors play an important role in present day microsystems. These microsystems are also required to accommodate electronics to harness raw signals into acceptable levels and also to make the signal insensitive to the effects of signals which are outside the domain of the system. Thus for instance, if a microsystem is realized for sensing and monitoring pressure, it should be able to track the effects of temperature and correct the output to compensate for the effect of temperature. The micromachined components of these microsystems are fragile structures and they are invariably exposed to harsh aggressive environments such as the corrosive water of the ocean which comes into contact with the pressure sensing microsystem used in oceanography. As a result, the packaging technology for microsystems plays a very important role in protecting these micro devices from the shock, the chemical environment and temperature extremities. In some biomedical applications such as intracranial pressure (ICP) and blood pressure monitoring sensors, the package should invariably be biocompatible. In aerospace applications which map the pressure in the aero foil, the package needs to be flat and should not exceed 1mm in height. The packaging technology for microsystems is thus more involved and varied than the packaging technology for integrated circuit chips. Here, we discuss the techniques used for packaging microsystems considering specific case of micromachined silicon piezoresistive pressure sensors.

12.2 The Importance and Challenges

MEMS pressure sensor packaging includes three major tasks, namely, (i) Assembly, (ii) Packaging and (iii) Testing, abbreviated as AP&T. The AP&T of microsystems contributes to a significant portion of the overall cost of production and could vary from 20% of the overall production cost with plastic passivation designed for a friendly environment in mass production, to as high as 95% of total cost for special pressure sensors for high temperature application with toxic-pressurizing media. Thus the AP&T cost for microsystems and especially for MEMS pressure sensors/ transducers varies from one product to another. Currently, this cost represents, on an average, 80% of the total production cost. The source of the failure of microsystems can be traced, in most cases, to inadequate packaging. As a result, microsystem packaging technology has become a key factor in MEMS product design and development, and it has attracted great interest and the attention of the microsystem community all over the world.

Packaging the micromachined component of the MEMS pressure transducer should be designed to meet the demands and requirements of the end user, whether those requirements be generic or specific. It consists of a complex matrix of solutions and is a multi disciplinary field, irrespective of whether it is an application driven or performance driven requirement. The reliable packaging of these devices and systems is a major challenge to the industry because microsystem of packaging has not reached the maturity level of its counterpart, the microelectronics packaging, has reached.

The packaging of the MEMS pressure transducer is required to protect the sensing or actuating elements when the sensing device is in contact with the medium, which, in itself, is the source of action, as in a gas sensor. Many media are hostile to these elements. The pressure sensor/ transducer packaging is highly challenging because the core devices of microsystems, such as micro-sensors usually involve delicate, complex three-dimensional geometry made of layers of dissimilar materials [Gardener, 1994; Malshe et al., 1999].

12.3 Functional Requirements

The mechanical package and its associated manufacturing technologies must fulfill functions like mechanical protection for day-to-day use in the service intended, and media protection when operated in harsh environments such as humidity, salt water, body fluids, fuels and gases etc. It should incorporate a convenient low cost means to interface and to isolate a very sensitive silicon die from undesirable mechanical stresses. The sensor package must be carefully designed to isolate the stress and reject extraneous mechanical straining inputs from any other variables such as acceleration, vibration etc. Simultaneously the package should allow the efficient transfer of the mechanical variable of desired inputs i.e., pressure in this case. Silicon, which is used for fabricating micro sensors and actuators, is a relatively low-expansion material while most packaging materials such as metals and ceramic exhibit considerably higher expansion. Hence, the package must allow for an appropriate means of reducing the undesirable effects of thermally-created stresses due to expansion or contraction.

An electrical interface is to be achieved by depositing and patterning aluminum or a noble metal thin film layer on the die. Modern silicon sensors often incorporate calibration and compensation either by using them on the silicon die itself or by employing hybrid components / signal conditioning ICs / resistors. The package must provide an appropriate means of incorporating and protecting these additional components. Hence the package provided must be suitable for housing and protecting the associated signal conditioning electronics.

In addition to the functional requirements that the package must accomplish, a suitable packaging scheme must have low cost, reliability, compatibility with subsequent assembly techniques and high volume production capability.

12.4 Microsystem Packaging Techniques

The packaging techniques used in silicon sensors originate from two distinct roots. One root is its adaptation from the well-established IC industry. The second major root of sensor packaging technology is derived from the conventional mechanical technology of aerospace and other process control industries. This excellent packaging technology involves the more traditional, reliable and well-established mechanical arts like machining (Precision CNC turning, milling, grinding, drilling, honing, polishing, Lapping, electro discharge machining etc.,), welding (Electron Beam Welding, Laser welding, precision TIG/MIG welding, Electric welding), Brazing (Vacuum Brazing and micro brazing), Engraving, metal etching, electro plating, anodizing, Glass to metal sealing, casting of alloys etc. The modern silicon sensor package is a blend or amalgamation of these two arts. Hence, to produce a package which is rugged and reliable, the silicon sensor-packaging engineer seeks to employ the best from each art.

Microsystems packaging is categorized into three levels, namely (i) die level, (ii) device level and (iii) system level as shown schematically [Hsu, 2002] in Figure 29. The primary objectives of **die level or wafer level packaging** are to protect the die or other core elements from plastic deformation or cracking; to protect the active circuitry for signal transduction of the system; to provide the necessary electrical and mechanical isolation of these elements and to ensure that the

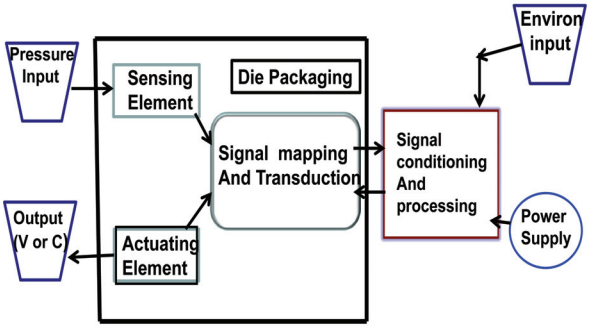

Fig. 29 Schematic representation of system packaging pressure transducer

system functions at both normal operating and overload conditions.

The major challenges in **device level packaging** are associated with interface requirements like the interface of delicate dice and core elements with other parts of the packaged product at radically different sizes. The interfaces of these delicate elements with the environment, particularly with regard to such factors as temperature, pressure and toxicity of the working and the contacting media are some of the critical issues to be addressed.

System level packaging involves the packaging of primary signal circuitry with the die or core element unit. System packaging requires proper mechanical and thermal isolation as well as electromagnetic shielding of the circuitry. Metal housing usually gives excellent protection from mechanical and electromagnetic influences. Assembly tolerance is a more serious problem at this level of packaging than at the device level [Hsu, 2002; Judy, 2001; Li & Tseng, 2001].

Figures 30(a) and (b) illustrate various headers required for absolute and gauge/relative MEMS pressure sensor packaging respectively. Figures 31(a) and 31(b) illustrate respectively the absolute pressure sensor header assembly and the gauge/ relative pressure sensor header assembly with provision for oil filling to isolate the silicon die from corrosive pressure media through a stainless steel diaphragm. The header assembly for a differential pressure sensor is illustrated in Figure 32. The die and wire bonded package suitable for dry gas media (No oil filling and no isolated stainless steel diaphragm) is shown in Figure 33. In this case, the pressure media is directly in contact with the silicon die. The packaging scheme required for various corrosive media, isolated by a stainless steel diaphragm with silicone oil in between, is shown in Figure 34

12.5. Microsystem Development at CeNSE in IISc Bangalore

Recently, we [Bhat & Nayak, 2012] have taken up activities on MEMS systems development at CeNSE in IISc, with the goal of achieving technological readiness for future Indian missions. Focused attention and efforts are needed to deliver

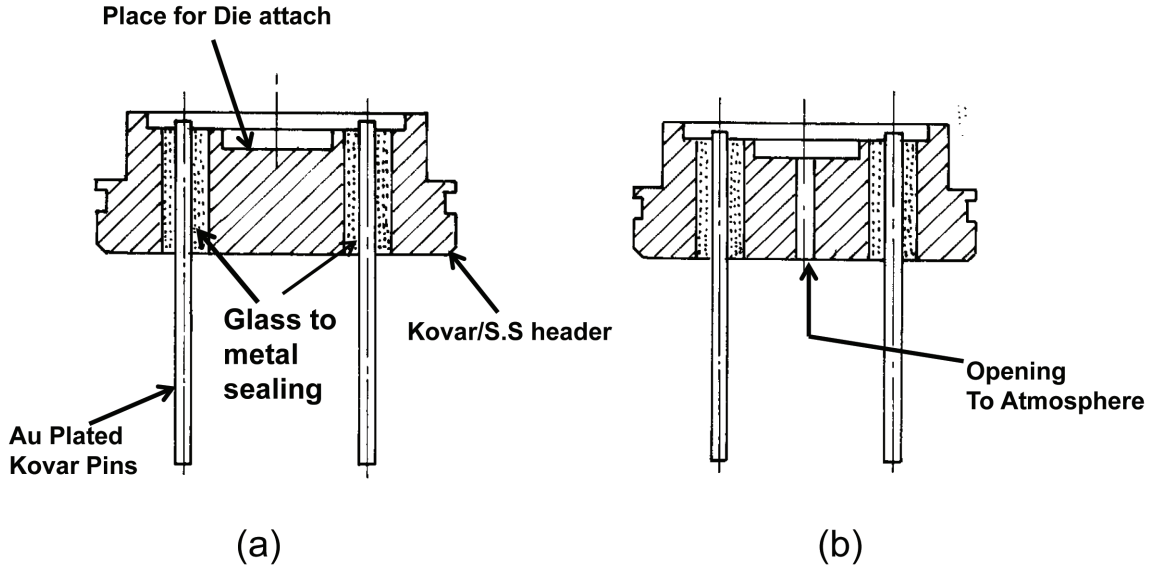

Fig. 30 Header assembly for (a) absolute pressure sensor (b) Gauge/relative pressure sensor

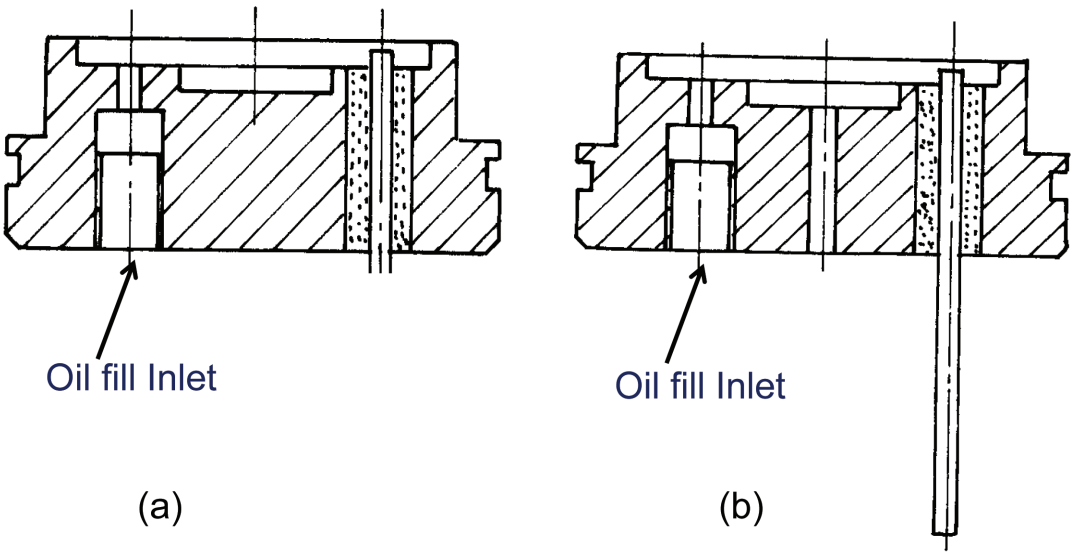

Fig. 31 Header Assembly with provision for oil filling for (a) Absolute Pressure sensor (b) Gauge/Relative Pressure Sensor

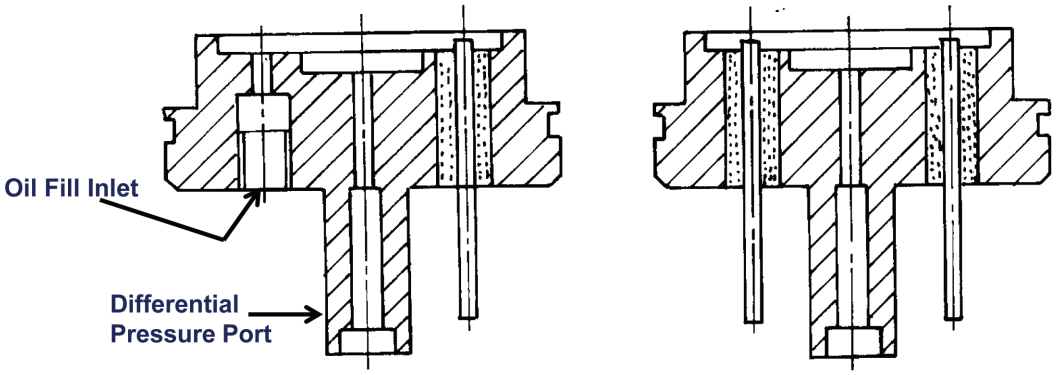

Fig. 32 Header Assembly for Differential Pressure Sensor (a) with provision for oil filling and extension for Evacuation /pressurization (b) with extension for easy evacuation/ pressurization.

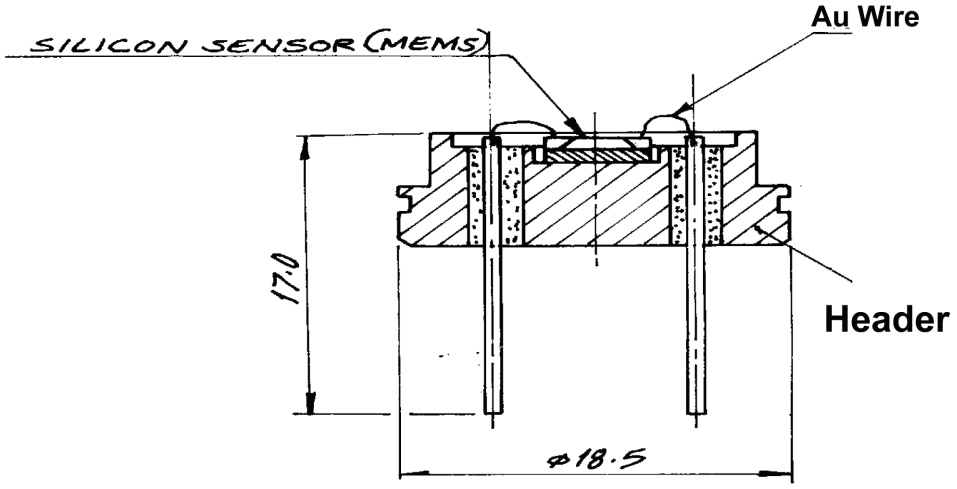

Fig. 33 The package suitable for dry gas media showing the die bonded and wire bonded pressure sensor

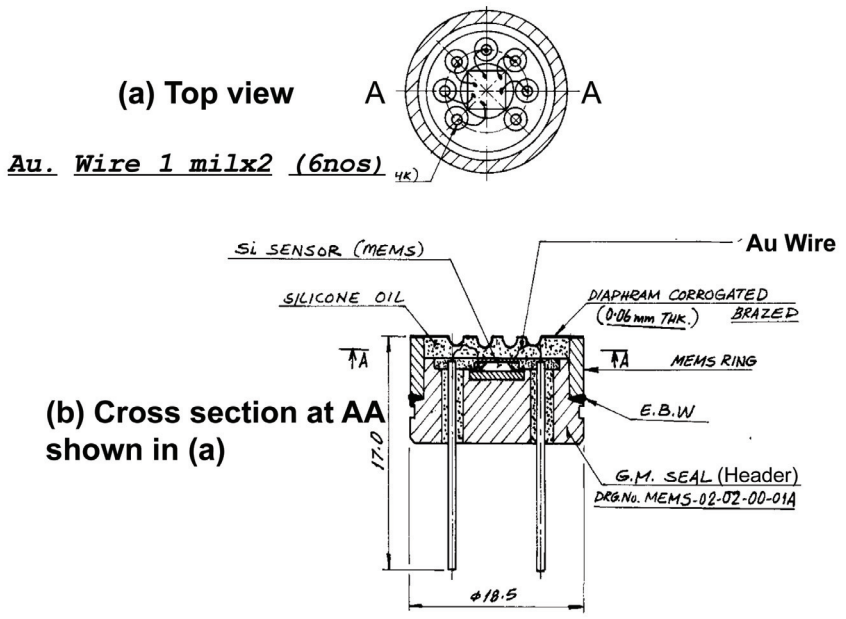

Fig. 34 Oil filled packaging scheme with stainless steel diaphragm. The wire bonded die mounted on the header is protected against corrosive media by the silicone oil between silicon die and the steel diaphragm .

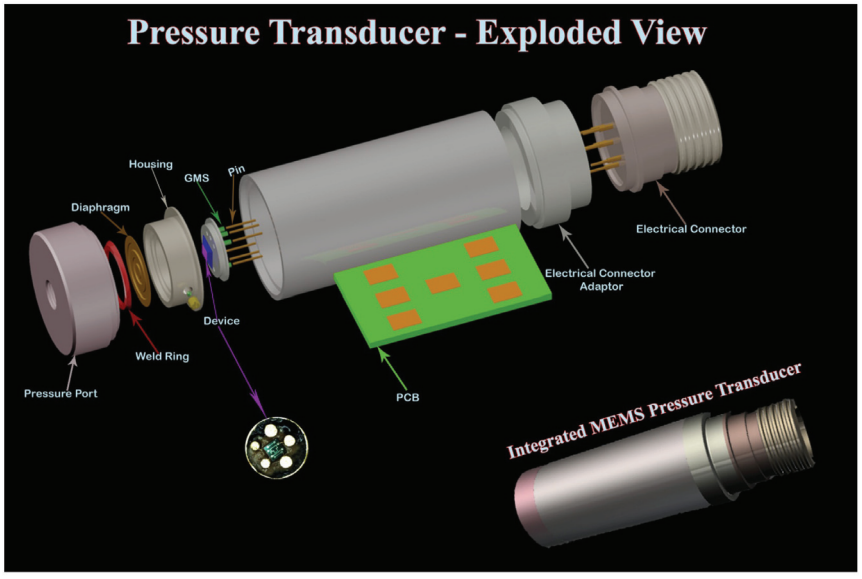

Fig. 35 Aerospace quality MEMS pressure transducer

MEMS-based systems. One such device viz., an aerospace quality MEMS pressure transducer, which is in an advanced stage of development, is illustrated in Figure 35. The set-up used for calibrating such sensors is shown in figure 36.

13 The Future and the Vision

The future is tending towards MEMS to Nano technology. Nano technology provides the ability to work at the molecular level, atom by atom, to create large structures with a fundamentally new molecular organization. The emerging approach for both chemical and biological MEMS sensors is based on carbon nanotube (CNT) and graphene-based technology. It is essentially concerned with materials, devices and systems to achieve structures and components which exhibit novel and significantly improved physical, chemical and biological properties, phenomena and processes due to their nano-scale size. These sensors have better sensitivity, selectivity and stability than commercially available sensors.

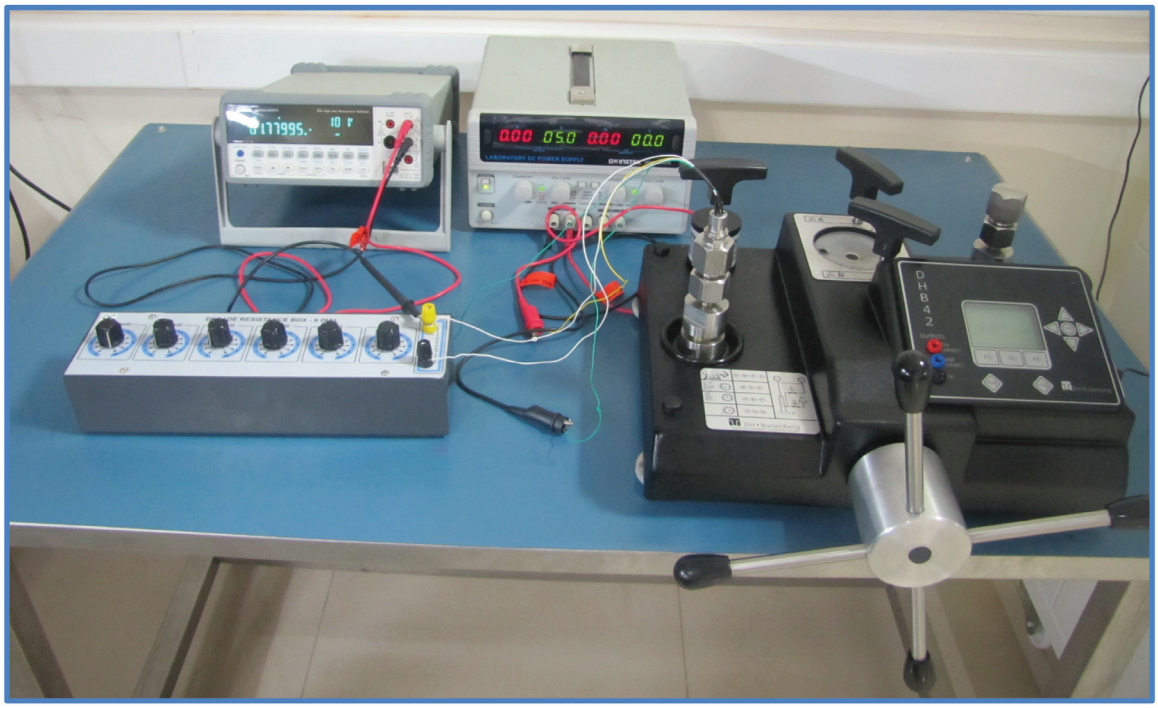

Fig. 36 Pressure transducer calibration setup

Focused R & D, with more attention and effort in design and packaging is needed in India to deliver MEMS-based devices to commercial as well as strategic programs. Effective collaborations between successful organizations may dramatically shorten the time frame between the concept to the systems. The following areas require careful attention and efforts:

- Polymer-clay, Nano-micro composite material for load bearing structures.
- Composite materials with embedded MEMS sensors.
- Nano and micro sensors and devices for space and terrestrial applications.
- MEMS based vibration sensing and analysis system for structural health monitoring
- Sensors for spacecraft structural health monitoring.
- Silicon on sapphire (SOS) based miniaturized sensors for high temperature operation in upto 30 °C for operation in harsh environment
- Silicon carbide (SiC) sensors for operation at temperatures in excess of 500°C and for operation in automotive applications as well as for corrosive fluids.

Acknowledgements

The authors are grateful to Dr V.K. Aatre, former Director General, Defence R&D, former SA to Raksha Mantri and the present chairman, BSMART of the National Program on Micro And Smart Systems (NPMASS) for his continued support and encouragement for many of the activities presented in this article which we carried out in the first phase (NPSM) and the second phase (NPMASS) of this National Program. The authors also gratefully acknowledge the support received from the Centre for Nano science and Engineering (CeNSE) at the Indian Institute of Science for carrying out the design, fabrication, packaging and characterization of these sensors. The authors also place on record the unconditional support received from Bharat Electronics Ltd Bangalore for several process steps such as the ion implantation of boron, dicing the devices from wafers and packaging the devices.

References

Bao M.-H., 2000, *Micro Mechanical Transducers: Pressure Sensors* Accelerometers *and Gyroscopes,* New York:Elsevier.

Bhat, K.N, P.R.S.Rao, Bhattachara,E., Dasgupta, A.,

Dasgupta, N., Vinoth Kumar, V., Sivakumar, K., Manjula, S.R., Madhavi, SP., Sushma,Y., & Daniel, R.J., 2005, "Micromachined polysilicon piezoresistive pressure sensor & accelerometer with SOI approach," *Electronics Today (India)*, pp.65-67.

Bhat, K.N.,Vinoth Kumar, V.,Sivakumar, K., Madhavi, S.P., DasGupta, A., Rao, P.R.S., ,Bhattacharya, E., DasGupta, N. Manjula, S.R., Daniel, R.J., & Natarajan, K., 2006 "Silicon Micromachining for MOS Integrated Piezoresistive pressure Sensors with SOI approach," *Indo-Japan Joint Seminar on 'Micro-Nano Manufacturing Science.* Tokyo, pp. 19 - 26.

Bhat, K.N. and Nayak, M.M. (Project coordinators) 2012, "Design, Fabrication, Packaging, Qualification Testing of Pressure sensors for Aerospace applications" This is a NPMASS sponsored project jointly taken up by CeNSE at IISc and BEL Bangalore with Rudra Pratap as PI, Navakanta Bhat, K.N.Bhat and M.M Nayak as Co-PIs from CeNSE; Y.P Prabhakara Rao, Kulkarni, Bharatidasan and Pramod, as Co-PIs from BEL. (June 2012-May 2014)

Du, J., Darrin J. Young, Christian A. Zorman, and Wen H. Ko, 2003, "Single Crystal SiC Capacitive Pressure Sensor at 400C ", IEEE Electron Device meeting (IEDM).

Fraga, M.A., Rodrigo Sávio Pessoa, Homero Santiago Maciel, Marcos Massi and Ivo de Castro Oliveira, 2010, "Technology roadmap for development of SiC sensors at plasma processes laboratory", J. Aerosp.Technol. Manag., São José dos Campos, Vol.2, No.2, pp. 219-224.

Fung, C. K. M. ,Zhang M Q. H. Zhang , Dong Z., and Li, W. J., 2005, "Fabrication of CNT-Based MEMS Piezoresistive Pressure Sensors Using DEP Nano assembly" *IEEE MEMS*, pp.251-254.

Gardener, J.W., 1994, *Microsensors –Principles and Applications*, London: John Wiley & Sons .

Hsu T.-R., 2002 *MEMS and Microsystems design and Manufacture.* Tata McGraw- Hill publishing Co. Ltd.

Judy, J. M. (2001) "Microelectromechanical systems (MEMS): Fabrication,Design and applications ", *Institute of Physics Publishing*. Vol. 10, pp 1115 – 1134.

Kovacs, G.T.A., 1998, Micromachined Transducers Source Book,New York, WCB McGraw-Hill

Li, G., and Tseng, A. A., 2001, "Low stress packaging of a Micromachined accelerometer," *IEEE Transactions on Electronics Packaging Manufacturing*, Vol.24, pp. 18-25, January.

Mallon J.R., Pourahmadi F.,Petersen K., Barth T.Vermeulen, and Brezek J., 1990, "Low Pressure Sensors employing bossed diaphragms and precision etch stopping," *Sensors and Actuators, Vol. A 21-A23*, pp. 89-95.

Malshe, A, etal., 1999, "Challenges in the packaging of MEMS " *Int. Journal of Microcircuits and Electronic packaging*. Vol 22, no:3,.

Manjula, S.R., 2005, "Optimization of Polysilicon Piezoresistors for MEMS Pressure Sensor," *M.S. Thesis.* Electrical Engineering Department, Indian Institute of Technology, Madras, India.

Meleshenko, V.V., 1997, "Bending of an elastic rectangular clamped plate: exact versus Engineering solutions," *J. Elasticity*, Vol. 48, pp.1-50.

Middlelhoek, S. & Audet, S.A., 1989, *Silicon Sensors* , San Diego, CA, Academic Press.

Mohamed, N. M., Lai M. K. and Begam K. M., 2010, "Development of Aligned Carbon Nanotubes (CNTs) for Pressure Sensing Application", NSTI-Nanotech, Vol.2, pp.130-133

Mosser,V., Susuki,J.,Goss,J, & Obermeier, E., 1991, "Piezoresistive Pressure Sensors Based on Polycrystalline Silicon," *Sensors and Actuators A,Vol.28,* pp 113-132.

Ned, A. A., Kurtz, A.D., Beheim, G., Masheeb, F., and Stefanescu, S., 2004) "Improved SiC Leadless Pressure Sensors For High Temperature, Low and High Pressure Applications", Kulite Semiconductor Products, Inc. Twenty-First Transducer Workshop Lexington, Maryland, June 22-23, 2004

Peterson, K.E., 1982*,* "Silicon as a mechanical material," *Proceedings of IEEE*, Vol. 70, 420-457

Raman, M. S., Kifle, T., Bhattacharya, E., & Bhat, K. N., 2006, "Physical Model for the Resistivity and Temperature Coefficient of Resistivity in Heavily Doped Polysilicon," *IEEE Transactions on Electron Devices , Vol53,* No.8, pp.1885-1892.

Smith, C., 1954, "Piezoresistance Effect in Germanium and Silicon," ***Physical Review*, Vol.94, pp 42–49**

Thyagarajan, V. R. and Bhat K.N., 2013, "Optimum location for Piezoresistors with Square Diaphragm

MEMS Pressure Sensors" (to be published).

Timoshenko, S. P., and S. Woinowski-Krieger, 1983, *Theory of Plates and Shells*, New York:McGraw-Hill.

Vandelli, N., 2008 "SiC MEMS Pressure Sensors For Harsh Environment Applications", MicroNano News , pp10-12 (April).

Vinoth Kumar, V., 2006 Design and Process Optimization for Monolithic Integration of Piezoresistive Pressure Sensor and MOSFET Amplifier with SOI Approach, *MS Thesis,* Electrical Engineering Department, Indian Institute of Technology, Madras, India.

Vinoth Kumar, V., A. DasGupta , K.N.Bhat and K. Natarajan, 2006, "Process Optimization for monolithic integration of piezoresistive pressure sensor and MOSFET Amplifier with SOI Approach," Journal of Physics Conference Series, Vol.34., pp. 210-215

Wong V.T.S. et al., 2000, "Bulk Carbon Nanotubes as Sensing Element for Temperature and Anemometry Micro Sensing", *Proc. IEEE MEMS 2003,* pp. 41-44,

Xiaowei,L., Xin, L., Wei, W., Xilian, W., Wei C., & Zhenmao, L., 1998,"Computer simulation of polysilicon piezoresistive pressure sensors," *IEE conference proceedings*, pp 891- 894.

Prof K.N.Bhat obtained his B.E degree in

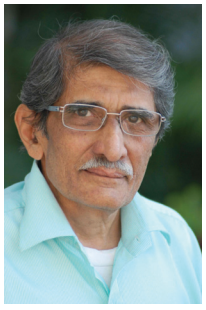

Electrical Engineering from the Indian Institute of Science Bangalore, Masters degree from the Rensselaer Polytechnic Institute (RPI) Troy NY and the PhD degree from the Indian Institute of Technology Madras. Subsequently, he did his post-doctoral research work at the RPI where he carried out extensive research work on the GaAs polycrystalline thin film solar cells and investigated the effects of grain boundary passivation on the GaAs polycrystalline solar cells. He has served as faculty member of the EE Department at IIT Madras at Chennai, India for nearly four decades and taught several courses both at the UG and PG levels on VLSI Technology, Semiconductor Power Devices, Compound Semiconductor Devices, Fundamentals of Semiconductor devices, and Basic Electronics circuits. He was evaluated by the students of IIT Madras as one of the top four best teachers across all the departments of the Institute. . His lecture series on High Speed Devices are now available in the youtube. He has also taught in the EE Department of the University of Washington at Seattle (USA) where he had spent a year on Sabbatical Leave and carried out exploratory research work along with Prof Robert Bruce Darling and realized Micro machined Faraday Cup Array Using Deep Reactive Ion Etching. He has guided several Ph.D and MS research scholars and published extensively in reputed International Journals and International Conference Proceedings. He has carried out pioneering work in the MEMS area in India and has coauthored the book entitled "Micro and Smart Systems–Technology and Modeling" published (2012) by John Wiley and Sons (USA). His book "Fundamentals of Semiconductor Devices" co-authored with Prof M.K. Achuthan, published (2007) by Tata McGgraw-Hill has been very popular all over the country.

Since 2006, he is a Visiting Professor at the Centre for Nano Science and Engineering, Indian Institute of Science Bangalore, after his superannuation and retirement from IITM. Prof K.N. Bhat is a Fellow of the Indian National Academy of Engineering

Dr. Manjunatha Nayak received D.IISc and

Ph.D. (Engg) degrees in Electronic Design Technology and Instrumentation respectively from IISc Bangalore. Subsequently he carried out his Post doctoral research in Micro Electro Mechanical Systems (MEMS) at University of Delft and Twente – Netherlands under INSA Invitation fellowship programme, and at Toyohashi University, Japan under JSPS fellowship.

He served in ISRO, Dept. of Space for nearly 40 years since 1971 in various capacities. He has grown professionally to Scientist/Engineer 'H' and held positions as Deputy Director, Semi-Conductor Laboratory, Chandigarh and Director, Launch Vehicle Programme Office, ISRO HQ Bangalore. During his 39 years of service at Liquid Propulsion

Systems Centre (LPSC) he has developed and productionised space qualified Pressure Transducers for PSLV, GSLV, IRS, INSAT, and Chandrayaan missions. The Ultrasonic liquid level sensors, depletion sensors and Temperature Sensors for the Launch vehicle programmes of ISRO, Digital Pressure Sensors for Automatic weather stations & Tsunami warning System were developed under his leadership and guidance. Various MEMS Sensors were designed, developed and fabricated with his guidance at SCL for Automotive, Radio Sonde, wind tunnel and Shock tube applications

In recognition of his outstanding contributions to ISRO's programmatic activities in various capacities, he was awarded ISRO MERIT Award in 2008. He has also received several other awards for his academic excellence. The best paper award in NSI-1989, SEP France Vikas Agreement Completion award in 1989, NRDC award in 1985, NPE- 1984 special award and Kirloskar Electric company best student award are only a few examples of such recognitions. He has more than 35 publications in refereed international journals, 4 patents and guided 7 Research students.

Superannuated from ISRO in June 2011, currently he is a Visiting Professor at Centre for Nano Science and Engineering, IISc, Bangalore, further pursuing his research activities in MEMS and Packaging. His research interests include MEMS and NEMS based sensors and actuators, and advanced MEMS packaging.

In recognition of his outstanding contributions to ISRO's programmatic activities in various capacities, he was awarded ISRO MERIT Award in 2008. He has also received several other awards for his academic excellence. The best paper award in NSI-1989, SEP France Vikas Agreement Completion award in 1989, NRDC award in 1985, NPE- 1984 special award and Kirloskar Electric company best student award are only a few examples of such recognitions. He has more than 35 publications in refereed international journals, 4 patents and guided 7 Research students.

Superannuated from ISRO in June 2011, currently he is a Visiting Professor at Centre for Nano Science and Engineering, IISc, Bangalore, further pursuing his research activities in MEMS and Packaging. His research interests include MEMS and NEMS based sensors and actuators, and advaned MEMS packaging.